New hydrocarbon trap models for the diagenetic transformation of opal-CT to quartz in Neogene siliceous rocks

Takashi Tsuji, Yasuhiro Masui, and Satoru Yokoi

ABSTRACT

Neogene siliceous rocks are known to act as both reservoirs and seals. However, the role of diagenetic alteration in the development of hydrocarbon reservoirs, seals, and traps in such formations is poorly understood. This study proposes two new models for hydrocarbon traps involving siliceous rock reservoirs with well-developed matrix porosity. The models are based on observations from the Yurihara and Toyotomi fields in Japan to evaluate changes in petrophysical properties associated with confining pressure and diagenetic transformations from opal-CT to quartz.

When this diagenetic transformation boundary is located at depths greater than approximately 1000 m (~3300 ft), the overlying opal-CT porcelanite layer forms a seal and the underlying clay-poor quartzose porcelanite forms a reservoir, facilitating the development of a hydrocarbon trap. The quartzose porcelanite containing less than 6% Al_2O_3 (an indication of clay content) can act as a reservoir even 1000 m (3300 ft) below the boundary.

When the boundary is located at depths shallower than approximately 500 m (~1650 ft), the overlying opal-CT porcelanite is unable to form a seal because of lower confining pressures—although clay-poor quartzose porcelanite continues to be a good reservoir. However, clay-rich quartzose porcelanite intercalated with the reservoir can act as a seal. When the quartzose porcelanite contains greater than 15% Al_2O_3, it has the potential to seal at the depth of the boundary. The requirement for a seal drops to greater than 8% Al_2O_3 at 1000 m (3300 ft) below the boundary.

Copyright ©2011. The American Association of Petroleum Geologists. All rights reserved.

Manuscript received November 27, 2009; provisional acceptance February 8, 2010; revised manuscript received May 5, 2010; final acceptance June 30, 2010.
DOI:10.1306/06301009192

AUTHORS

TAKASHI TSUJI ~ *Japan Petroleum Exploration Co., Ltd. (JAPEX) Research Center, 1-2-1, Hamada, Mihama-ku, Chiba, 261-0025, Japan; takashi.tsuji@japex.co.jp*

Takashi Tsuji received his B.S. degree from Okayama University in 1980 and his Ph.D. from Kyushu University in 1997. His main research focus is currently on the modeling of the Athabasca oil sands reservoirs using three-dimensional seismic data and multiple-point geostatistics. He is also particularly interested in shale-gas reservoirs.

YASUHIRO MASUI ~ *Japan Petroleum Exploration Co., Ltd. (JAPEX), Sapia Tower, 1-7-12, Marunouchi, Chiyoda-ku, Tokyo, 100-0005, Japan; yasuhiro.masui@japex.co.jp*

Yasuhiro Masui is a general manager of the Overseas Exploration Department for JAPEX. He joined JAPEX after graduating from Hokkaido University in 1979 with a B.S. degree in geology.

SATORU YOKOI ~ *Japan Petroleum Exploration Co., Ltd. (JAPEX), Sapia Tower, 1-7-12, Marunouchi, Chiyoda-ku, Tokyo, 100-0005, Japan; satoru.yokoi@japex.co.jp*

Satoru Yokoi received his B.S. degree in geology from the University of Kyoto in 1980. He joined JAPEX and is the general manager of the Domestic Exploration Department. He works on conventional hydrocarbon systems, which include fractured-basement reservoir, volcanic rocks reservoir, and oil-generating coal. He has also worked on unconventional shale-oil and shale-gas hydrocarbon systems since 1987.

ACKNOWLEDGEMENTS

We thank INPEX Corporation, Godo Shigen Sangyo Co., Ltd., the Toyotomi Town for permission to disclose geologic data of the Toyotomi R-2 and Ohmagari R-1, and the Japan National Oil Corporation (presently, Japan Oil, Gas and Metals National Corporation) for using CMS 200. We acknowledge Hakuyu Okada and Yoshikazu Aoki (emeritus professors of Kyushu University) and Ryuji Tada (University of Tokyo) for the support of and the critical review of a previous version of the manuscript. We also thank Japan Petroleum Exploration Co., Ltd. (JAPEX), for permission to publish this article and the

following colleagues for their help and participation in this project: Seijyuro Maiya, Yukio Ikuji, Kunio Kai, Osamu Takano, Mitsuru Inaba, Minoru Kuniyasu, Amane Waseda, Hideki Nishita, Shinho Habuki, Kenji Takagi, Mitsuru Kamon, Shinji Ijima, and Yuichi Saito. We are grateful to the following colleagues for assistance in analyzing samples: Yoshio Yasuda, Masahiko Yagi, Toshie Kazama, Teruo Suzaki, Tokujiro Takayama, Takashi Takahashi, Hideaki Ishii, Hisako Fujisaki, Mitsuko Sekiguchi, Chieko Koga, Mitsunao Kuramochi, Gennosuke Hirano, Chiyoko Sugawara, Hideko Sakai, and Kyoko Kosugi. We are grateful to Hikaru Fukazawa, Kazukiko Tezuka, Kazuyoshi Hoshi, Fumio Akiba, and Yutaka Yanagimoto (JAPEX) for stimulating discussions and helpful reviews of a previous version of the manuscript. Special thanks should be given to Yasuo Yamada (JAPEX), who provided continuous support and reviewed all versions of the manuscript. We would have found it almost impossible to finish this article without help from all these people and organizations. We also thank the AAPG editors G. M. Gillis and A. Sharrer and reviewers T. N. Diggs and M. W. Longman for review comments and technical support on the draft manuscript. The AAPG Editor thanks the following editors for their work on this paper: Tim Diggs and Mark W. Longman.

EDITOR'S NOTE

A color version of Figure 12 may be seen in the online version of this article.

Such traps have not been reported outside Japan; therefore, these models are likely to be useful for hydrocarbon exploration in siliceous rock formations elsewhere, such as in the Monterey Formation of California.

INTRODUCTION

Neogene siliceous rocks are known to host several proven oil and gas fields such as those found in the lower to middle Miocene Monterey Formation of central California. The reservoirs can be broadly divided into two lithologic types: chert and porcelanite (Table 1) (Schwalbach et al., 2004). Chert reservoirs tend to develop in coastal and offshore sedimentary basins such as the Santa Barbara–Ventura Basin, whereas porcelanite reservoirs are generally found in inland basins such as the San Joaquin Basin (Chaika and Williams, 2001; Schwalbach et al., 2004). Chert reservoirs, being highly fractured and having a low matrix porosity, can produce high-viscosity oil at rates as high as thousands of barrels per day. By contrast, porcelanite reservoirs have high matrix porosity and are only weakly fractured; such reservoirs commonly require fracturing to achieve production rates exceeding 500 bbl/day (80 kL/day) (Schwalbach et al., 2004). The U.S. Geological Survey (1974) reported property changes of porcelanites with silica mineral recrystallization, noting that recrystallization increases the size and improves the communication of pores, thereby permitting the accumulation of hydrocarbons.

Similar middle to upper Miocene siliceous rock reservoirs are also found in Japan (Sato et al., 1979; Sato and Annaka, 1986; Masui and Tsuji, 1990; Tsuji and Masui, 1992; Tsuji and Yokoi, 1994). The hydrocarbons in these fields are hosted mainly in quartzose porcelanite. Tada and Iijima (1983) showed that the matrix pores in porcelanite increase in diameter during the diagenetic silica-phase transformation from opal-CT to quartz, especially when the porcelanite has low clay content, but that this process is accompanied by a gradual decrease in porosity as a result of mechanical compaction.

Masui and Tsuji (1990) and Tsuji and Masui (1992) concluded that the transformation from opal-CT to quartz is closely related to the formation of hydrocarbon traps. In these studies of the porcelanite-dominated Onnagawa Formation of the Yurihara oil and gas field in northeast Japan, they reported that the opal-CT porcelanite located immediately above the transformation boundary forms a seal, whereas the quartzose porcelanite located immediately below the boundary forms reservoirs.

Table 1. Characteristics of Siliceous Rocks in This Study

	Siliceous Rock	
	Porcelanite	Chert
Luster-fresh surface	Matte	Glassy, waxy
Fracture character	Rough	Conchoidal
Color	Brownish gray–olive gray	Brownish black

Tsuji and Yokoi (1994) measured the distribution of pore-throat radii in porcelanite core samples within the porcelanite-dominated Masuporo and Wakkanai formations, in the Toyotomi area of northern Japan. The authors reported that the area where the hydrocarbons are trapped is not immediately below the boundary, where the pore-throat radii in quartzose porcelanite abruptly increase to almost maximum values, but rather at greater depths, where the quartzose porcelanite has a lower clay content than that found in surrounding layers.

Siliceous rock reservoirs in Japan consist of quartzose porcelanite with a highly porous matrix that resemble the reservoirs in the Monterey Formation developed in inland basins; however, few studies have investigated the relationship between the hydrocarbon traps in the Monterey Formation and the opal-CT to quartz transformation boundary, and the detailed properties of the reservoirs there remain mostly unreported. Furthermore, few studies of siliceous rock reservoirs in countries other than the United States exist (Rogers and Longman, 2001). The study by Tsuji and Yokoi (1994) is the only one to offer a detailed discussion of the reservoir properties of Japanese porcelanites.

In this study, we provide details about the relationship between hydrocarbon traps and the opal-CT to quartz transformation in the siliceous rock of the Yurihara field (Figure 1A). We have analyzed the siliceous rock and classified it into several lithologic types based on its appearance and the degree of burial diagenesis. We also measured the clay mineral content, permeability, porosity, and distribution of pore-throat radii, and documented the nature of the pore textures. We then examined the relationship between these properties and the occurrence of hydrocarbon shows or hydrocarbon production zones, and reinterpreted the physical properties of the siliceous rock from the Toyotomi area (Figure 1B) reported by Tsuji and Yokoi (1994). On the basis of these interpretations, we propose two new models for hydrocarbon trap development in siliceous rock and discuss the contribution of fractures to such traps as well as the applicability of siliceous rock reservoir classifications (Chaika and Williams, 2001).

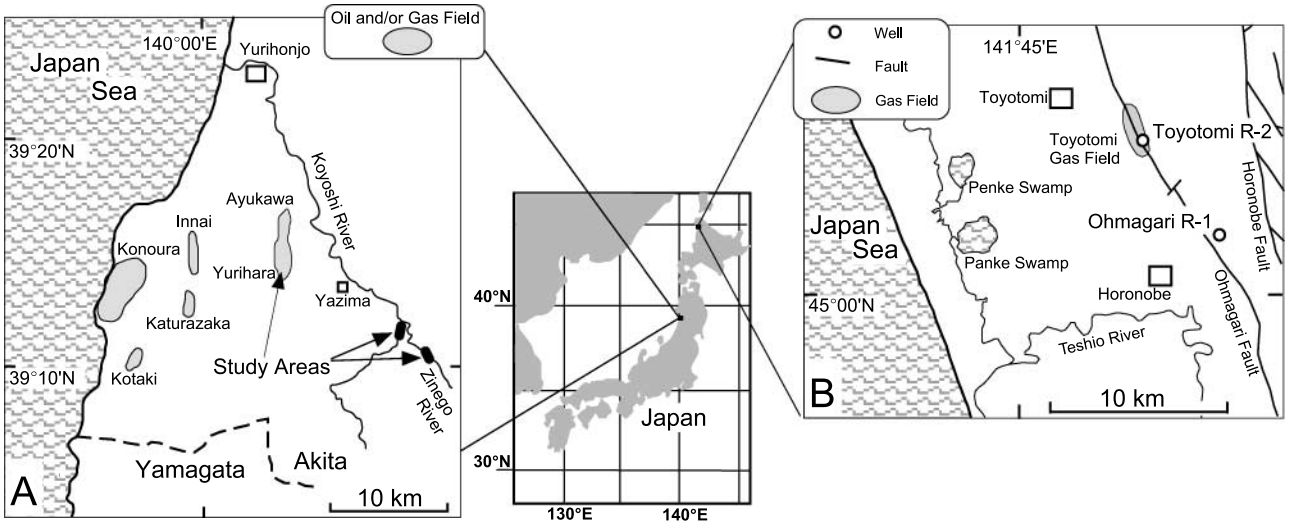

Figure 1. Index map (center) showing the Yurihara oil and gas field and neighboring outcrops (A) and the Toyotomi area (B). Distributions of oil and gas fields are from Japan Natural Gas Association and Japan Offshore Petroleum Development Association (1982). Name and distribution of faults are from Nagano (1960).

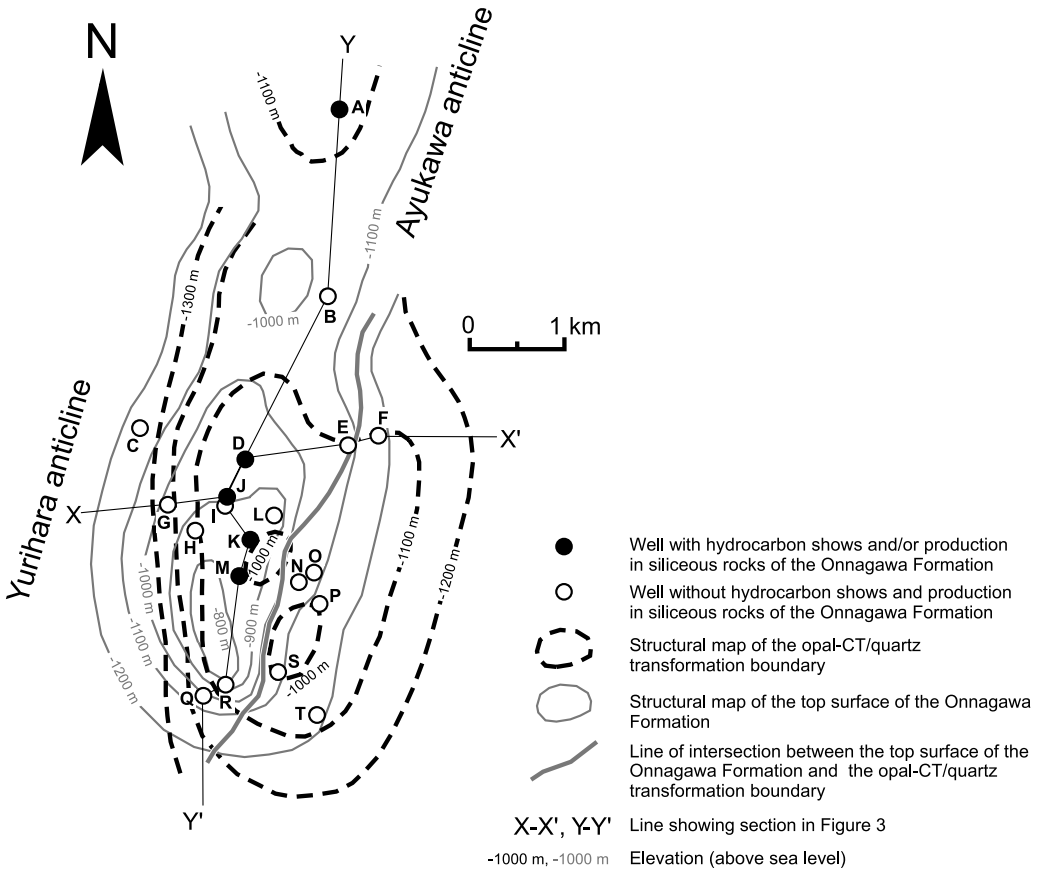

Figure 2. Structure map of the top surface of the Onnagawa Formation and the opal-CT to quartz diagenetic transformation boundary in the Yurihara oil and gas field.

BACKGROUND GEOLOGY

Regional Setting

The rim of the northern Pacific is marked by widespread accumulations of Neogene siliceous rock such as the lower to middle Miocene Monterey Formation in California (Garrison, 1975) and the upper middle Miocene to middle upper Miocene Onnagawa Formation in Japan (Iijima and Tada, 1981).

The sedimentary basins of the Onnagawa Formation are believed to have developed in connection with the opening of the Sea of Japan. During the late early Miocene to the early middle Miocene, the rapid opening and deepening of the sea formed the northeast rift of the deep-sea basin (Iijima, 1992). This in turn created an inflow of the Kuroshio warm current from the southwestern corner of the sea, resulting in the deposition of mudstone during the Nishikurosawa stage. At this time, the lowermost basin fill, represented by the "Green Tuff formation" of the Nishikurosawa stage, was formed by active acid and basic submarine volcanism (Iijima, 1992). The opening of the Sea of Japan slowed then stopped during the late middle Miocene to early late Miocene. At that time, the southwestern entrance of the sea was closed by an isthmus, suspending the inflow of the Kuroshio warm current and allowing the inflow of the Oyashio cold current from the north to dominate (Iijima, 1992). Accordingly, the Onnagawa Formation was deposited in the northeast rift of the deep-sea basin (Iijima, 1992; Shiraishi and Matoba, 1992), consisting mainly of siliceous rock (e.g., siliceous mudstone, porcelanite, and chert) locally interbedded with layers of acid to intermediate tuff. The proportion of argillaceous clastics in the siliceous rock gradually increases and grades into the massive mudstones of the middle-to-late upper Miocene Funakawa Formation (Shiraishi and Matoba, 1992).

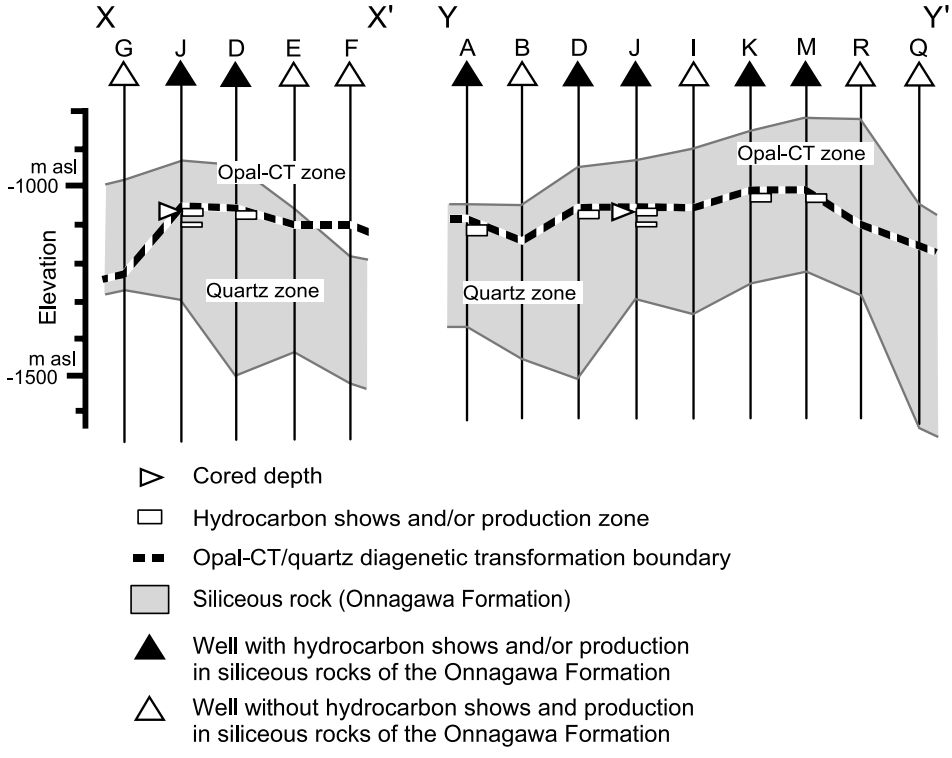

Figure 3. Stratigraphic cross sections across the Yurihara oil and gas field (see Figure 2 for the locations of the cross sections), showing the relationships among the Onnagawa Formation (composed of siliceous rocks), the opal-CT to quartz diagenetic transformation boundary, and hydrocarbon shows and production horizons. asl = above sea level.

Yurihara Oil and Gas Field

The Yurihara oil and gas field is located approximately 15 km (~9 mi) south of Yurihonjo City, Akita Prefecture, Japan (Figure 1A). It occupies the north-south–trending Yurihara anticline within a 300- to 800-m (1000- to 2600-ft)-thick succession of the Onnagawa Formation and the underlying Green Tuff formation. The Yurihara anticline, along with several other north-south–trending folds and faults in the region, developed simultaneously with the deposition of the Funakawa Formation, and remains active (Ozawa et al., 1988).

The main reservoirs in the Yurihara field are the (1) basalts (i.e., lavas and hyaloclastite) and (2) acid tuffs of the Green Tuff formation. The field was discovered in the early 1980s, and production began in the mid-1980s (Inaba, 2001). During the drilling for these deep targets, siliceous rock of the Onnagawa Formation was encountered, yielding hydrocarbon shows referred to as noncommercial "shale gas."

Exploration in the Yurihara field started near the culmination of the anticline, where wells M, R, and Q were drilled (Figures 2, 3). The first production test in the siliceous rocks of the Onnagawa Formation was conducted in well D and produced 23,000 m^3 (817 mcf) gas/day. Further tests for the same horizon at two intervals in well J produced 43,000 m^3 (1527 mcf) gas/day and 16 kL (100 bbl) oil/day in the upper and lower intervals, respectively (Araki and Kato, 1993). Within the upper interval, a single suite of cores (well J core) was obtained. The exploration subsequently shifted to the north toward the Ayukawa anticline. Well A was drilled at the saddle between the anticlines; it produced 57,000 m^3 (2024 mcf) gas/day and 2 kL (13 bbl) oil/day from siliceous rocks (Araki and Kato, 1993).

SAMPLES AND STUDY METHODS

Samples

We analyzed cuttings from 20 wells (Figure 2, wells A–T) in addition to the well J core and outcrop samples collected in the vicinity of the Yurihara field. On the basis of appearance (Table 1), most

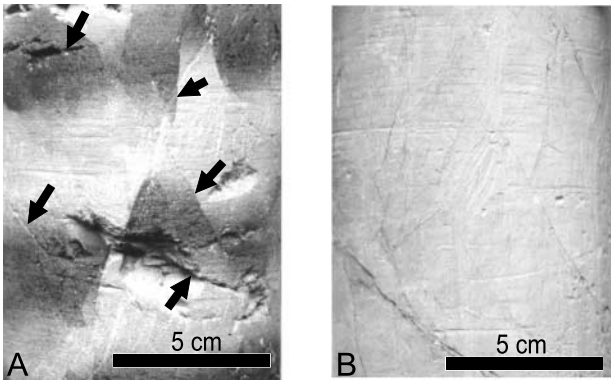

Figure 4. Representative porcelanite core collected from well J in the Yurihara field. (A) Alternating beds of porcelanite (light colored: brownish gray) and chert (dark colored: brownish black). Oil shows were observed in the matrix of the porcelanite and along open fractures recognized in both the chert and porcelanite. Arrows are pointing at open fractures. (B) Olive gray porcelanite without hydrocarbon shows and open fractures.

of the samples were classified as porcelanite and the rest as chert.

Cutting samples of porcelanite from the Onnagawa Formation were taken at 20-m (66-ft) intervals from each well, which resulted in 114 samples. The well J core, collected at a depth interval of 1310 to 1318 m (4300–4325 ft) (–1054 to –1062 m above sea level [asl] [–3458 to –3484 ft asl]), consists of brownish gray and olive gray porcelanites, brownish black cherts, and minor tuffs. The cherts alternate with the brownish gray porcelanites on a scale of 3 to 5 cm (1.2–2 in.) (Figure 4A). Over this interval, hydrocarbon shows have been confirmed only in the brownish gray porcelanites and tuffs. Open fractures occur in both the cherts and the brownish gray porcelanites (Figure 4A), and they are especially well developed in the former. Hydrocarbon shows have also been identified along these fractures, but the olive gray porcelanites, which are characterized by closed and healed fractures (Figure 4B), contain no hydrocarbon shows. The well J core yielded five porcelanite samples with hydrocarbon shows (no. 11–13, 15, and 16) and one without (no. 17). Two chert samples (no. 20 and 21) were also collected from the well J core. Thirteen samples (no. 1–10, 14, 18, and 19) were obtained from outcrops of porcelanite within the Onnagawa Formation exposed along the Koyoshi River and Zinego River, approximately 10 km (~6 mi) southeast of the Yurihara oil and gas field (Figure 1A). Note that, unless otherwise specified, we hereinafter use the ground level for the datum when referring to depth.

Sample Lithology

We subdivided the samples of porcelanite and chert into three lithologic types on the basis of the degree of burial diagenesis: opal-CT porcelanite, quartzose porcelanite, and quartzose chert. To determine the degree of burial diagenesis of the samples, we used powder x-ray diffraction to quantify the biogenic silica (opal-CT). This permitted the discrimination between siliceous rocks containing opal-CT (opal-CT siliceous rocks) and those containing only quartz (quartzose siliceous rocks). As the depth increases, the opal-CT content increasingly transforms to quartz. We will refer to the depth at which that transformation is complete as the opal-CT to quartz diagenetic transformation boundary.

We used a Rigaku Geigerflex 4012 x-ray diffractometer to analyze the mineral composition of the samples. After being dried at 60°C, the samples were pulverized and mounted on an aluminum plate with a 20-mm (0.8-in.)-wide hole. Measurements were taken with the following settings: a radiation source of CuKα; acceleration voltage of 40 kV; beam current of 35 mA; three slits of 1, 0.15, and 1°; scanning range of 2θ between 2.5 and 50°; and scanning speed of 2°/min.

Clay Mineral Content

Because the features of pores within siliceous rock depend not only on the degree of burial diagenesis, but also on the clay mineral content (Iijima and Tada, 1981; Goter et al., 1992; Tsuji and Yokoi, 1994; Chaika and Williams, 2001; Reid and McIntyre, 2001a), we also examined the clay mineral content in each sample. The clay mineral content was estimated from whole-rock chemical compositions. The Miocene siliceous rock consists of a mixture of diatom tests of nearly pure silica and argillaceous

clastics (Tada, 1991b). Because argillaceous clastics generally contain clay minerals at a known ratio, the Al_2O_3 content can be used as an index of the amount of clay mineral content in the siliceous rock.

Whole-rock chemical compositions were determined with a Rigaku IKF 3070 x-ray fluorescence spectrometer using an Rh target (45 kV, 30 mA). The concentrations of 10 major elements were determined through an analysis of glass beads that had been prepared by fusing a mixture of 0.35 g of rock powder dried at 60°C with 3.5 g of lithium tetraborate dried at 1200°C for 5 min.

Porosity and Permeability

We measured porosity and permeability using a CoreLab CMS 200 with each plug core of sample. Plug cores were prepared with diameters of 2.5 cm (1 in.) and lengths of 2 to 3 cm (0.8–1.2 in.), with the long axis parallel to the bedding plane. Visible fractures were avoided as much as possible, but several visible fractures less than 0.1 mm (0.004 in.) in width were observed in two of the plug cores (no. 12 and 15). None of these fractures extended across the entire plug core. The bulk volumes of the plug cores were measured by mercury immersion, followed by drying in a vacuum. Using nitrogen gas, we measured the porosity and permeability of the plug cores set in the CMS 200 under two effective confining pressures (800 psi [5.5 MPa] and either 1200 or 2300 psi [8.3 or 15.9 MPa]) to simulate subsurface conditions. The lower pressure represented the minimum confining pressure set by this apparatus, and higher pressures were chosen to be close to 1120 psi (7.7 MPa), the effective confining pressure at the gas-producing depth in well J, or double this value. We refer to the measured porosity as Φ_{CMS} to distinguish it from the porosity obtained by the measurement of the distribution of pore-throat radii, subsequently described.

Distribution of Pore-Throat Radii, Bulk Density, and Grain Density

The distributions of pore-throat radii, bulk densities, and grain densities were measured using a mercury injection porosimeter (CarloErba P 220). We analyzed individual rock fragments of approximately 7 mm diameter after drying them at 60°C for 2 days. For the porcelanite samples from the Toyotomi area, the pore-throat radii tend to fall in two ranges, either less than 0.02 μm or between 0.02 and 0.15 μm (Tsuji and Yokoi, 1994). We classified the measured pore-throat radii into three groups: (1) throat-S (<0.02 μm, small), (2) throat-M (0.02–0.15 μm, medium), and (3) throat-L (≥0.15 μm, large). The purpose of dividing them in this way was to reveal the distribution characteristics of the pore-throat radii for each lithologic type. Partial porosities arising from pores in these three groups are referred to as throat-S porosity, throat-M porosity, and throat-L porosity. The total porosity will be referred to as Φ_{Hg}.

Observations of Rock Texture

We observed rock textures on polished and/or artificial fractured surfaces that were oriented normal to bedding using a scanning electron microscope (SEM) of a thousand times magnification (1000×).

Number of Samples

We identified the mineral phases of silica in all 135 samples. The results obtained from cutting samples were used to identify the opal-CT to quartz transformation boundary in each well. We determined whole-rock chemical compositions and distributions of pore-throat radii for 21 samples that came from either the well J core or surface outcrops. We measured permeability for 13 samples from the well J core and the surface outcrops (but not for the chert, which was too fractured to allow the preparation of plug cores). With the exception of the chert, we observed textural features with representative petrophysical properties.

Reexamination of Data from the Toyotomi Area

The data described so far were not sufficient for a comprehensive analysis of hydrocarbon traps in siliceous rock because the only data we had on the distribution of pore-throat radii in the Yurihara field

Table 2. Petrophysical Properties and Major Element Composition of Siliceous Rocks from the Toyotomi Area

Well Name	Diagenetic Silica Phase	Sample No.	Depth (m)	Lithology	Bulk Density (g/cm^3)	Grain Density (g/cm^3)	Distribution of Pore-Throat Radii* MPR (μm)	Modal Pattern	Porosity (ϕ_{Hg}) (%) Total	S	M	L	M + L
Toyotomi R-2	Opal-CT	1	149	Porcelanite	1.46	2.30	0.011	Bimodal	37	23	13	1	13
		2	172	Porcelanite	1.56	2.24	0.012	Bimodal	30	21	8	1	9
		3	188	Porcelanite	1.38	1.96	0.017	Bimodal	29	15	13	1	14
		4	199	Porcelanite	1.37	2.31	0.009	Bimodal	41	27	12	1	13
		5	222	Porcelanite	1.56	2.22	0.012	Bimodal	30	27	2	1	3
		6	233	Porcelanite	1.57	2.21	0.011	Bimodal	29	21	7	1	8
		7	252	Porcelanite	1.41	2.15	0.009	Bimodal	35	25	9	1	10
		8	267	Porcelanite	1.66	2.30	0.011	Bimodal	28	24	3	1	4
		9	279	Porcelanite	1.52	2.25	0.010	Bimodal	32	22	8	2	10
		10	315	Porcelanite			0.012	Bimodal	29	19	9	1	9
		11	332	Porcelanite	1.63	2.24	0.011	Bimodal	27	22	5	1	6
		12	362	Porcelanite	1.62	2.26	0.011	Bimodal	28	19	7	2	9
		13	413	Porcelanite	1.37	2.36	0.012	Bimodal	42	29	12	1	13
		14	481	Porcelanite	1.45	2.42	0.012	Unimodal	40	36	4	0	4
		15	499	Porcelanite	1.40	2.33	0.011	Unimodal	40	38	2	0	2
		16	512	Porcelanite	1.58	2.42	0.012	Unimodal	35	32	2	1	3
		17	552	Porcelanite	1.63	2.47	0.015	Unimodal	34	32	1	1	2
		18	552	Porcelanite	1.41	2.31	0.013	Unimodal	39	34	5	0	5
	Quartzose	19	564	Porcelanite	1.67	2.50	0.070	Unimodal	33	7	23	3	27
		20	603	Porcelanite	1.74	2.46	0.075	Unimodal	29	5	23	1	24
		21	643	Porcelanite	1.77	2.55	0.060	Unimodal	31	7	17	7	24
		22	670	Porcelanite	1.96	2.52	0.036	Unimodal	22	9	10	3	13
		23	702	Porcelanite	1.81	2.45	0.055	Unimodal	26	6	19	2	20
		24	731	Porcelanite	1.71	2.45	0.109	Unimodal	30	4	15	11	26
		25	753	Porcelanite	1.90	2.57	0.024	Unimodal	26	11	13	2	15
		26	786	Porcelanite	1.67	2.39	0.129	Unimodal	30	3	15	13	28
		27	800	Porcelanite	1.77	2.39	0.095	Unimodal	26	5	20	2	22
		28	804	Porcelanite	1.85	2.46	0.097	Unimodal	25	4	19	1	21
		29	804	Porcelanite	1.75	2.46	0.136	Unimodal	29	3	13	13	25
Ohmagari R-1	Opal-CT	1	247	Porcelanite	1.68	2.40	0.012	Bimodal	30	23	5	2	7
		2	340	Porcelanite	1.48	2.26	0.012	Bimodal	35	28	6	1	7
		3	380	Porcelanite	1.35	2.37	0.012	Bimodal	43	36	6	1	7
		4	397	Porcelanite	1.25	2.36	0.016	Bimodal	47	31	15	1	16
		5	404	Porcelanite	1.25	2.36	0.015	Bimodal	47	34	13	1	13
		6	447	Porcelanite	1.70	2.43	0.019	Unimodal	30	24	4	2	6
	Quartzose	7	495	Porcelanite	1.55	2.53	0.115	Unimodal	39	5	20	13	33
		8	547	Porcelanite	1.72	2.49	0.090	Unimodal	31	5	23	3	26
		9	588	Porcelanite	1.91	2.61	0.089	Unimodal	27	4	21	2	23
		10	653	Porcelanite	1.94	2.49	0.040	Unimodal	22	6	15	1	16
		11	705	Porcelanite	2.03	2.46	0.022	Unimodal	18	8	9	1	10
		12	754	Porcelanite	1.91	2.51	0.034	Unimodal	24	8	15	1	16
		13	802	Porcelanite	2.00	2.49	0.030	Unimodal	20	7	11	1	12
		14	849	Porcelanite	1.91	2.55	0.051	Unimodal	25	6	19	1	20
		15	896	Porcelanite	1.76	2.31	0.095	Unimodal	24	4	19	1	20

Chemical Composition (%)											
SiO_2	TiO_2	Al_2O_3	Fe_2O_3	MnO	MgO	CaO	Na_2O	K_2O	P_2O_5	LOI**	Total (%)
75.43	0.42	8.67	3.19	0.03	1.33	0.44	1.54	1.47	0.07	7.96	100.55
72.84	0.47	9.67	3.65	0.03	1.42	0.42	1.48	1.65	0.07	8.82	100.52
77.37	0.37	7.43	2.84	0.02	1.14	0.39	1.37	1.33	0.07	7.79	100.12
77.16	0.36	7.59	2.68	0.02	1.04	0.35	1.43	1.25	0.06	7.90	99.84
74.91	0.43	8.92	3.20	0.02	1.29	0.29	1.52	1.53	0.05	8.43	100.59
73.02	0.48	9.70	3.84	0.03	1.43	0.33	1.55	1.71	0.06	8.79	100.94
79.37	0.33	6.77	2.47	0.02	0.89	0.29	1.26	1.20	0.05	7.64	100.29
72.26	0.47	9.47	3.83	0.03	1.32	0.43	1.51	1.71	0.08	8.36	99.47
76.05	0.42	8.35	3.30	0.02	1.05	0.37	1.49	1.47	0.06	8.49	101.07
75.07	0.45	9.05	3.45	0.02	1.04	0.37	1.60	1.60	0.06	8.41	101.12
74.13	0.46	9.68	3.34	0.02	1.23	0.39	1.71	1.63	0.08	8.35	101.02
73.37	0.46	9.48	3.44	0.02	1.15	0.38	1.49	1.68	0.06	8.61	100.14
78.51	0.37	7.42	2.68	0.03	0.97	0.37	1.47	1.33	0.06	6.90	100.11
77.96	0.36	7.52	2.91	0.02	1.05	0.36	1.39	1.31	0.05	8.40	101.33
82.62	0.27	5.66	2.07	0.02	0.70	0.31	1.23	1.00	0.04	6.35	100.27
74.99	0.39	7.97	3.15	0.03	1.16	0.40	1.39	1.44	0.06	8.21	99.19
75.53	0.42	8.41	3.24	0.03	1.12	0.54	1.57	1.58	0.06	7.92	100.42
78.06	0.33	6.87	2.67	0.02	0.97	0.41	1.34	1.28	0.05	7.10	99.10
71.18	0.52	10.27	3.68	0.03	1.58	0.48	1.69	1.85	0.06	8.10	99.44
74.16	0.48	9.61	3.65	0.03	1.53	0.61	1.77	1.70	0.08	7.00	100.62
71.47	0.51	10.21	3.73	0.03	1.40	0.30	1.63	1.84	0.06	8.58	99.76
73.59	0.48	9.45	3.43	0.03	1.22	0.33	1.49	1.70	0.06	8.87	100.65
74.09	0.43	8.68	3.23	0.03	1.13	0.30	1.37	1.55	0.06	8.71	99.58
77.83	0.37	7.16	2.77	0.02	0.85	0.29	1.25	1.23	0.07	9.09	100.93
67.16	0.59	12.23	4.74	0.04	1.62	0.40	1.67	2.06	0.07	10.31	100.89
81.10	0.30	6.41	2.33	0.02	0.73	0.22	0.94	1.03	0.04	7.79	100.91
79.39	0.36	7.49	2.59	0.02	0.09	0.29	1.02	1.31	0.05	7.81	100.42
80.07	0.36	7.08	2.62	0.02	0.78	0.32	1.11	1.27	0.05	7.61	101.29
81.76	0.29	6.25	2.18	0.02	0.72	0.27	1.00	1.06	0.04	6.64	100.23
70.56	0.54	11.24	3.79	0.03	1.25	0.43	1.56	1.93	0.06	8.55	99.94
76.20	0.42	8.82	3.19	0.02	0.98	0.34	1.49	1.53	0.05	8.11	101.15
80.79	0.29	6.33	2.60	0.02	0.75	0.31	1.18	1.07	0.04	7.12	100.50
79.40	0.33	7.08	2.61	0.02	0.83	0.36	1.26	1.26	0.04	7.24	100.43
81.95	0.28	5.89	2.32	0.02	0.67	0.30	1.18	1.01	0.04	6.25	99.91
73.57	0.49	9.94	3.85	0.03	1.23	0.56	1.52	1.69	0.06	8.25	101.19
75.61	0.43	8.55	3.29	0.03	1.06	0.44	1.38	1.48	0.06	8.12	100.45
80.68	0.34	6.92	2.71	0.02	0.79	0.33	1.28	1.21	0.04	7.32	101.64
78.97	0.34	6.95	2.71	0.02	0.81	0.31	1.16	1.22	0.04	7.27	99.80
79.16	0.37	7.85	2.57	0.02	0.96	0.33	1.23	1.25	0.04	6.82	100.60
75.48	0.43	8.74	3.28	0.03	1.13	0.40	1.25	1.56	0.05	7.04	99.39
77.46	0.46	9.67	3.35	0.03	1.25	0.44	1.64	1.69	0.06	7.28	103.33
75.95	0.45	8.96	3.28	0.03	1.16	0.40	1.34	1.66	0.05	6.67	99.95
78.59	0.37	7.50	2.85	0.02	0.90	0.34	1.20	1.34	0.05	7.24	100.40
81.78	0.33	6.82	2.68	0.02	0.91	0.38	1.08	1.19	0.05	5.26	100.50

Table 2. Continued

Well Name	Diagenetic Silica Phase	Sample No.	Depth (m)	Lithology	Bulk Density (g/cm^3)	Grain Density (g/cm^3)	Distribution of Pore-Throat Radii* MPR (μm)	Modal Pattern	Porosity (ϕ_{Hg}) (%) Total	S	M	L	M + L
Ohmagari R-1	Quartzose	16	935	Porcelanite	1.86	2.46	0.081	Unimodal	24	5	18	1	19
		17	956	Porcelanite	1.91	2.56	0.050	Unimodal	25	6	18	1	19
		18	958	Porcelanite	1.78	2.47	0.075	Unimodal	28	5	20	2	23
		19	975	Porcelanite	1.95	2.48	0.059	Unimodal	21	5	14	2	16
		20	1055	Porcelanite	1.89	2.42	0.045	Unimodal	22	6	15	0	16
		21	1109	Porcelanite	1.88	2.54	0.048	Unimodal	26	7	17	2	19
		22	1153	Porcelanite	1.90	2.40	0.064	Unimodal	21	5	14	1	15
		23	1205	Porcelanite	1.88	2.51	0.076	Unimodal	25	4	20	1	21
		24	1253	Porcelanite	1.93	2.31	0.033	Unimodal	17	5	10	1	12
		25	1351	Porcelanite	2.05	2.46	0.028	Unimodal	17	6	9	2	11
		26	1404	Porcelanite	1.77	2.48	0.195	Unimodal	28	2	7	19	26
		27	1496	Porcelanite	2.04	2.48	0.037	Unimodal	18	5	12	1	13
		28	1571	Porcelanite	2.26	2.57	0.010	Unimodal	12	9	1	2	3
		29	1693	Porcelanite	2.27	2.63	0.016	Unimodal	14	9	3	2	5
		30	1762	Porcelanite	1.90	2.44	0.066	Unimodal	22	2	19	0	20
		31	1939	Porcelanite	2.36	2.68	0.011	Unimodal	12	9	2	1	3

*MPR = median pore-throat radius; S = porosity defined by throat-S pores; M = porosity defined by throat-M pores; L = porosity defined by throat-L pores; M + L = porosity defined by throat-M and throat-L pores.
**LOI = loss on ignition.

were from the well J core. In particular, we required data that covered a greater range of depths. Therefore, we reexamined data from the Toyotomi area (Tsuji and Yokoi, 1994) to the north (see Figure 1 for location) using the same criteria used in this study for the Yurihara field.

In the Toyotomi area, the Masuporo Formation (middle Miocene) is unconformably overlain by the Wakkanai Formation (uppermost middle Miocene to lower upper Miocene), which conformably grades upward into the Koetoi Formation (upper upper Miocene to lower Pliocene) and the Yuchi and Sarabetu formations (upper Pliocene to Pleistocene) (Fukusawa et al., 1992). Siliceous rock, which is almost continuous within the Masuporo and Wakkanai formations, forms the major reservoirs (Tsuji and Yokoi, 1994). These formations are correlated with the Onnagawa Formation, not only by their lithology, but also by their depositional age.

Tsuji and Yokoi (1994) examined the rock properties of porcelanites in two wells: Toyotomi R-2 in the Toyotomi gas field and Ohmagari R-1 located 7 km (4.3 mi) to the southeast (Figure 1B). Cores were retrieved throughout the entire depth range of each well. Siliceous rocks in the Masuporo and Wakkanai formations in these wells consist almost completely of porcelanites. Data regarding the mineral phase of biogenic silica, whole-rock chemical composition, and the distribution of pore-throat radii can be found in Tsuji and Yokoi (1994) (Table 2). In this study, we also provide data on the bulk and grain densities (Table 2) obtained while measuring the distribution of the pore-throat radii.

In the Toyotomi area, the opal-CT to quartz transformation boundary is located at a depth of approximately 500 m (~1650 ft) (Tsuji and Yokoi, 1994), which is shallower than the boundary estimated from the geothermal gradient of 2.3°C/100 m in this area (Japan Natural Gas Association and Japan Offshore Petroleum Development Association, 1982) and from the opal-CT to quartz transformational temperature of 69°C that has been widely observed in wells in Japan (Aoyagi and

Chemical Composition (%)											
SiO_2	TiO_2	Al_2O_3	Fe_2O_3	MnO	MgO	CaO	Na_2O	K_2O	P_2O_5	LOI**	Total (%)
78.76	0.38	7.62	2.80	0.02	1.00	0.40	1.05	1.39	0.05	6.73	100.20
78.10	0.39	8.23	2.96	0.02	1.10	0.38	1.21	1.41	0.05	7.27	101.12
78.25	0.40	8.21	2.88	0.02	1.11	0.40	1.31	1.38	0.04	7.81	101.81
77.35	0.40	7.89	3.09	0.02	0.93	0.41	1.31	1.48	0.07	7.48	100.43
79.35	0.36	7.69	2.75	0.02	0.95	0.35	1.07	1.31	0.04	8.31	102.20
78.69	0.42	8.44	2.88	0.02	1.09	0.35	1.09	1.43	0.04	6.96	101.41
79.82	0.35	7.02	2.52	0.02	0.84	0.38	0.88	1.28	0.04	8.02	101.17
82.35	0.30	6.08	2.14	0.01	0.70	0.37	0.76	1.06	0.03	7.37	101.17
78.54	0.34	6.89	2.74	0.01	0.80	0.47	0.81	1.12	0.03	8.61	100.36
78.38	0.34	6.94	2.62	0.01	0.83	0.45	0.76	1.21	0.04	9.89	101.47
88.85	0.16	3.81	1.30	0.01	0.43	0.29	0.47	0.69	0.03	5.30	101.34
80.93	0.27	5.96	2.34	0.01	0.75	0.33	0.71	1.04	0.03	8.59	100.96
75.29	0.40	7.87	3.13	0.02	1.04	0.39	1.11	1.26	0.05	9.06	99.62
73.42	0.45	8.95	3.39	0.02	1.28	0.63	1.46	1.33	0.06	9.88	100.87
80.63	0.25	6.19	2.29	0.02	0.81	0.45	1.10	0.91	0.06	7.78	100.49
65.85	0.59	12.56	5.38	0.04	2.13	0.37	2.07	2.26	0.07	9.35	100.67

Kazama, 1980). Because the two wells in the Toyotomi area are located in the hanging wall of the Ohmagari fault (a reverse fault), we assume that the boundary formed before thrusting and has since been uplifted along the fault (Tsuji and Yokoi, 1994).

PETROPHYSICAL PROPERTIES OF THE SILICEOUS ROCKS

Lithology and Whole-Rock Chemical Composition

In this section, we consider only samples from the well J core and the surface outcrops; the cutting samples are considered in the section on hydrocarbon occurrences. Of the 21 samples, we classified 10 as opal-CT porcelanite, 9 as quartzose porcelanite, and 2 as quartzose chert (Table 3).

Table 3 lists the whole-rock chemical compositions of each sample. The Al_2O_3 content has a moderate to strong positive correlation with the TiO_2, Fe_2O_3, MgO, and Na_2O contents (r^2 = 0.54–0.78) and a strong negative correlation with the SiO_2 content (r^2 = 0.87). The regression line for SiO_2 versus Al_2O_3 passes through the point where SiO_2 = 95% and Al_2O_3 = 0%, which is consistent with the assumption that siliceous rock represents a mixture of diatom tests of nearly pure silica and argillaceous clastics. Al_2O_3 content was 3.27 to 9.02% (average, 5.85%) for opal-CT porcelanite, 3.17 to 9.49% (average, 5.89%) for quartzose porcelanite, and 5.75 to 5.77% (average, 5.76%) for quartzose chert. Because the opal-CT porcelanite and quartzose porcelanite have similar Al_2O_3 values, we conclude that they also have similar clay mineral contents.

Porosity, Bulk and Grain Densities, and Distribution of Pore-Throat Radii

Data on the porosity, bulk density, and grain density of the siliceous rock samples are shown in Tables 3 and 4 and Figure 5. The average bulk density of

Table 3. Petrophysical Properties and Major Element Compositions of Siliceous Rocks from the Yurihara Oil and Gas Field and Neighboring Outcrops

Diagenetic Silica Phase	Sample No.	Locality	Lithology	Bulk Density (g/cm^3)	Grain Density (g/cm^3)	Distribution of Pore-Throat Radii*									
						MPR (μm)	Modal Pattern	Porosity (ϕ_{Hg}) (%)					Porosity (ϕ_{CMS}) (%)		
								Total	S	M	L	L + M	800 psi	1200 psi	2300 psi
Opal-CT	1	Koyoshi R.	Porcelanite	1.02	1.82	0.018	Bimodal	44	23	17	4	21			
	2	Koyoshi R.	Porcelanite	1.25	2.31	0.012	Bimodal	46	29	16	1	17	45.3		45.0
	3	Koyoshi R.	Porcelanite	1.25	2.24	0.013	Bimodal	44	29	14	1	15			
	4	Koyoshi R.	Porcelanite	1.36	2.41	0.013	Bimodal	44	29	14	1	15			
	5	Koyoshi R.	Porcelanite	1.44	2.37	0.013	Unimodal	39	36	3	0	3	38.8		38.6
	6	Koyoshi R.	Porcelanite	1.42	2.24	0.011	Unimodal	37	35	1	1	2	37.0	37.0	
	7	Koyoshi R.	Porcelanite	1.51	2.27	0.009	Unimodal	34	32	1	1	2	35.4	35.4	
	8	Koyoshi R.	Porcelanite	1.60	2.47	0.012	Unimodal	35	31	3	1	4	34.9		34.5
	9	Koyoshi R.	Porcelanite	1.75	2.49	0.011	Unimodal	30	28	1	1	2	30.7	30.6	
	10	Koyoshi R.	Porcelanite	1.41	2.43	0.014	Unimodal	42	37	5	0	5			
Quartzose	11	Well J	Porcelanite	1.58	2.60	0.256	Unimodal	39	2	8	29	37			
	12	Well J	Porcelanite	1.59	2.47	0.244	Unimodal	35	1	9	25	34	32.4	32.2	
	13	Well J	Porcelanite	1.61	2.58	0.209	Unimodal	38	3	11	24	35	35.8	35.7	
	14	Zinego R.	Porcelanite	1.67	2.58	0.185	Unimodal	35	2	11	22	33	34.7		34.4
	15	Well J	Porcelanite	1.61	2.48	0.148	Unimodal	35	3	15	17	32	23.6	23.4	
	16	Well J	Porcelanite	1.80	2.58	0.223	Unimodal	30	3	6	21	27	18.8	18.6	
	17	Well J	Porcelanite	1.75	2.59	0.071	Unimodal	32	5	26	1	27			
	18	Koyoshi R.	Porcelanite	1.90	2.50	0.051	Unimodal	24	7	18	0	18	26.5	26.5	
	19	Koyoshi R.	Porcelanite	1.97	2.68	0.043	Unimodal	27	8	17	2	19	26.4		26.1
	20	Well J	Chert	2.27	2.49	0.015	Unimodal	9	7	2	0	2			
	21	Well J	Chert	2.38	2.45	0.010	Unimodal	3	3	0	0	0			

*MPR = median pore-throat radius; S = porosity defined by throat-S pores; M = porosity defined by throat-M pores; L = porosity defined by throat-L pores; M + L = porosity defined by throat-M and throat-L pores.

opal-CT porcelanites (1.40 g/cm^3) is lower than that of quartzose porcelanites (1.72 g/cm^3); the average bulk density of quartzose porcelanites is lower than that of quartzose cherts (2.33 g/cm^3) (Tables 3, 4). The average ϕ_{CMS} and ϕ_{Hg} of the opal-CT porcelanites (37.0 and 39%, respectively) are higher than those of quartzose porcelanites (28.3 and 33%, respectively), and the ϕ_{Hg} values of the quartzose porcelanites are higher than those of the quartzose cherts (6%). The large increase in the effective confining pressure from 800 to 1200 or 2300 psi (5.5–8.3 or 15.9 MPa) causes only a minor decrease in ϕ_{CMS} (up to 1%; see Table 3; Figure 5). The ϕ_{CMS} and ϕ_{Hg} are almost identical in the individual samples, except for the two samples of quartzose porcelanites (no. 15 and 16), in which the total porosities (ϕ_{Hg}), 35% and 30%, respectively, are approximately 50% higher than their ϕ_{CMS} (Table 3).

Tables 3 and 4 and Figure 6 show the distributions of pore-throat radii in the siliceous rocks. We observe unimodal and bimodal distributions among the opal-CT porcelanites (Figure 6A). Six samples (no. 5–10) display a unimodal distribution, and four samples (no. 1–4) display a bimodal distribution. However, the unimodal and bimodal distribution groups have mostly similar median pore radii (average, 0.012 and 0.014 μm, respectively) because both of them are characterized by a majority of throat-S porosity. The latter group contains throat-M and throat-L pores in addition to throat-S pores.

Permeability (md)			Chemical Composition (wt. %)									
800 psi	1200 psi	2300 psi	SiO_2	TiO_2	Al_2O_3	Fe_2O_3	MnO	MgO	CaO	Na_2O	K_2O	P_2O_5	Total
			79.50	0.26	6.05	1.20	0.01	0.40	0.32	0.46	1.69	0.14	90.03
<0.001		<0.001	82.51	0.19	4.70	1.29	0.01	0.56	0.93	0.39	1.07	0.12	91.77
			82.80	0.19	5.06	1.24	0.01	0.57	0.92	0.38	1.20	0.13	92.50
			81.19	0.20	4.63	1.28	0.02	0.51	0.78	0.29	1.08	0.10	90.08
<0.001		<0.001	82.96	0.21	5.16	1.21	0.01	0.49	0.28	0.30	0.92	0.04	91.58
0.36	0.16		83.10	0.22	5.26	1.54	0.02	0.46	0.37	0.38	0.81	0.03	92.19
0.49	0.09		86.15	0.13	3.27	0.91	0.01	0.25	0.24	0.22	0.55	0.03	91.76
<0.001		<0.001	72.13	0.42	9.02	2.68	0.03	0.70	0.92	0.80	1.91	0.12	88.73
0.12	0.06		77.85	0.24	6.73	2.05	0.02	0.76	0.82	0.62	0.93	0.18	90.20
			72.30	0.37	8.61	2.51	0.02	0.59	0.41	0.62	2.33	0.14	87.90
			82.75	0.14	4.21	1.25	0.01	0.13	0.07	0.50	2.33	0.05	91.44
4.0	3.5		85.46	0.10	3.17	0.85	0.02	0.09	0.10	0.32	1.80	0.05	91.96
1.4	1.3		77.62	0.20	5.65	1.53	0.02	0.24	0.11	0.55	3.04	0.06	89.02
0.76		0.72	84.22	0.22	5.21	1.26	0.01	0.26	0.18	0.26	1.03	0.10	92.75
2.9	2.1		78.94	0.18	5.46	1.50	0.03	0.27	0.15	0.45	2.93	0.09	90.00
1.1	1.1		84.82	0.13	3.68	0.87	0.01	0.08	0.06	0.31	2.20	0.04	92.20
			74.71	0.24	9.49	1.68	0.03	0.68	0.50	1.52	3.05	0.09	91.99
0.07	0.06		76.36	0.28	7.08	2.11	0.02	0.88	0.50	0.47	1.08	0.08	88.86
0.045		0.04	72.81	0.40	9.08	3.67	0.10	1.30	1.21	0.64	1.47	0.22	90.90
			78.43	0.21	5.75	1.61	0.03	0.19	0.13	0.41	3.66	0.07	90.49
			79.06	0.18	5.77	1.41	0.02	0.14	0.11	0.43	3.81	0.06	90.99

The distribution of pore-throat radii in quartzose porcelanites is characterized by a large amount of throat-L porosity and a small amount of throat-S porosity; this distribution obviously differs from that for opal-CT porcelanites. The distribution for quartzose porcelanites is unimodal, and the median pore-throat radius (average, 0.159 μm) is much larger than that for opal-CT porcelanites. Pores in quartzose cherts are mainly throat-S type, and the median pore-throat radii for this (average, 0.012 μm) are similar to those for opal-CT porcelanites.

Permeability

Table 3 and Figure 7 show the permeabilities of the porcelanites measured under various confining pressures. The permeabilities of opal-CT porcelanites are, in general, lower than those of quartzose porcelanites. In particular, the permeabilities of three samples of opal-CT porcelanite (no. 2, 5, and 8) are below the measurable limit (0.001 md) of the measuring device at the minimum confining pressure of 800 psi (5.5 MPa). The permeabilities of the three other samples of opal-CT porcelanite (no. 6, 7, and 9) decreased sharply (by 50–80%) in response to an increase in the confining pressure from 800 to 1200 psi (5.5–8.3 MPa).

In contrast, the permeabilities of the quartzose porcelanites showed little decrease (by 0–30%) when the effective confining pressure was increased to 1200 or 2300 psi (8.3 or 15.9 MPa). The quartzose porcelanites can be divided into two groups according to their permeabilities: group A, with permeabilities greater than 0.7 md, and group B, with

Table 4. Summary of the Petrophysical Properties of Siliceous Rocks from the Yurihara Oil and Gas Field and Neighboring Outcrops*

	Siliceous Rock				
	Opal-CT Porcelanite			Quartzose Porcelanite	Quartzose Chert
	Unimodal**	Average	Bimodal**		
Porosity (ϕ_{CMS})†		37.0%† (6) 39%†† (10)		28.3%† (7)	Not measured†
(ϕ_{Hg})††	35.4%† (5) 36%†† (6)		45.3%† (1) 45%†† (4)	33%†† (9)	6%†† (2)
Bulk density (g/cm^3)	1.22 (6)	1.40 (10)	1.52 (4)	1.72 (9)	2.33 (2)
Grain density (g/cm^3)	2.20 (6)	2.31 (10)	2.38 (4)	2.56 (9)	2.47 (2)
Median pore-throat radius (μm)	0.012 (6)	0.012 (10)	0.014 (4)	0.159 (9)	0.012 (2)
Porosity (ϕ_{Hg}) defined by throat-L pores	1% (6)		2% (4)	16% (9)	0% (2)
Porosity (ϕ_{Hg}) defined by throat-M pores	2% (6)		15% (4)	13% (9)	1% (2)
Porosity (ϕ_{Hg}) defined by throat-S pores	33% (6)		28% (4)	4% (9)	5% (2)
Porosity (ϕ_{Hg}) defined by throat-M + L pores	3% (6)		17% (4)	29% (9)	1% (2)
Permeability	<0.001–0.49 md (5)‡		<0.001 md (1)‡	0.045–4.0 md (7)‡	Not measured

*Values in parentheses denote number of samples.
**Distribution pattern of pore-throat-radii.
†Porosity measured using a CoreLab CMS 200 under an effective confining pressure of 800 psi (5.5 MPa).
††Porosity measured by the mercury injection method.
‡Permeability measured using a CoreLab CMS 200 under an effective confining pressure of 800 psi (5.5 MPa).

permeabilities less than 0.1 md (Figure 7). The samples in group B show lower permeabilities than some of opal-CT porcelanite samples (no. 6, 7, and 9). The samples in group A contain a lower Al_2O_3 content (average, 4.63%) than those in group B (average, 8.08%). The group A samples with the highest (no. 12) and second highest permeabilities (no. 15) contain open fractures. Even if these two samples are excluded, group A still shows higher permeability than group B.

Rock Textures

We examined the rock texture of four porcelanite samples: two opal-CT porcelanite samples with bimodal and unimodal distributions of the pore-throat radii, and two quartzose porcelanite samples with low and high Al_2O_3 contents (Figure 8). The polished surface of the opal-CT porcelanite with a bimodal distribution of pore-throat radii (no. 1; Al_2O_3 = 6.05%) shows scattered pores (diameter, 1–10 μm) that occupy approximately 10% of the surface area (Figure 8A). A fractured surface of this sample shows irregularly shaped pores (diameter, 10–50 μm), some of which appear to be interconnected in three dimensions (Figure 8B). In contrast, as Figure 8C (polished surface) and 8D (fractured surface) show, few pores are evident in the opal-CT porcelanite with a unimodal distribution of pore-throat radii (no. 5; Al_2O_3 = 5.16%), and the pores are clearly isolated from each other. No clay minerals are evident inside the pores within the examined opal-CT porcelanites.

The quartzose porcelanites exhibit more pores than the opal-CT porcelanites do. The polished surface of the low-Al_2O_3 quartzose porcelanite (no. 11; Al_2O_3 = 4.21%) contains large scattered pores (diameter, 5–10 μm) connected to a network of trench-shaped pores with widths of several microns (Figure 8E). Most of the fractured surfaces are covered with aggregates of subhedral quartz (diameter, 1–2 μm) with intercrystalline pores (Figure 8F).

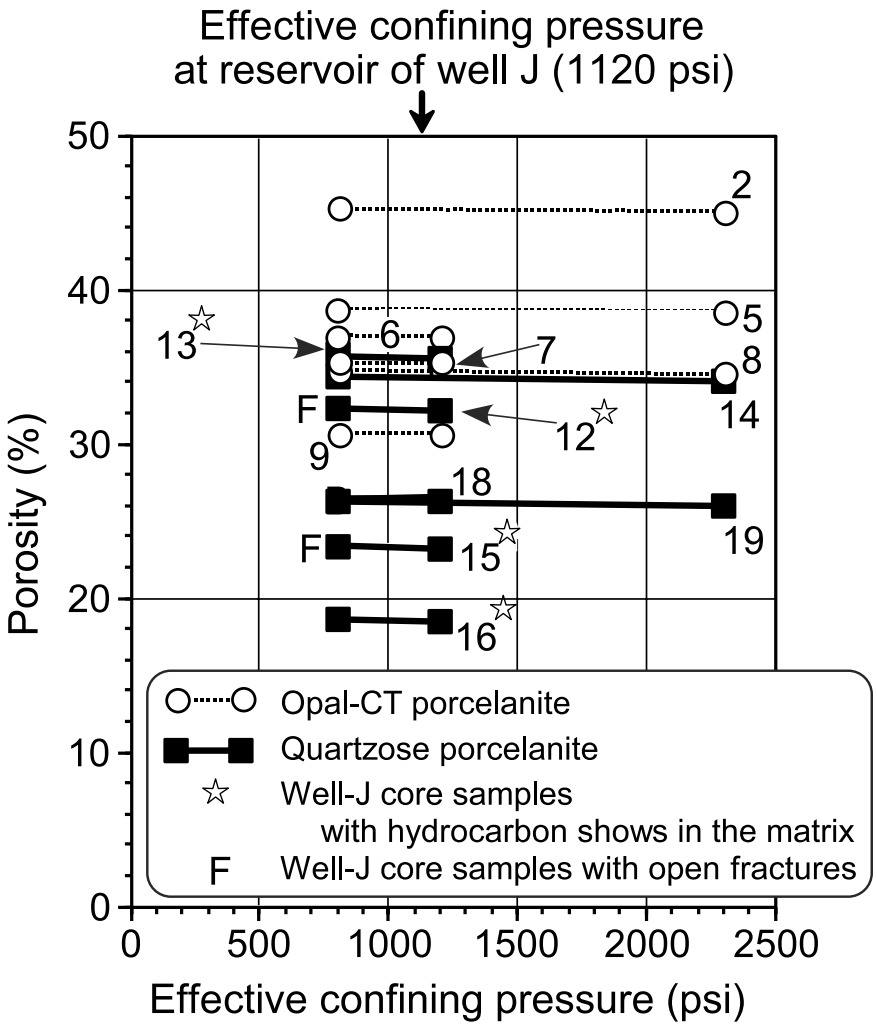

Figure 5. Relationship between porosity and effective confining pressure for porcelanite. The number on each line corresponds to the sample numbers listed in Table 3.

On the fractured surface of the high-Al_2O_3 porcelanite (no. 17; Al_2O_3 = 9.49%), we observed aggregates of subhedral quartz, as with the low Al_2O_3 variety (no. 11), among which are pores that contain clay mineral grains of several microns in diameter (Figure 8G).

HYDROCARBON OCCURRENCES

Figure 2 shows a structural map of the top surface of the Onnagawa Formation and the opal-CT to quartz transformation boundary, and Figure 3 shows the relationship between these two surfaces and the hydrocarbon shows and hydrocarbon-producing zones. The transformation boundary is clearly not concordant with the top of the Onnagawa Formation. Zones of both hydrocarbon production and hydrocarbon shows tend to occur just below the transformation boundary, which forms the culmination in the Onnagawa Formation. In other words, they occur at the culmination of the quartzose porcelanite within the Onnagawa Formation.

The occurrence of hydrocarbon shows in the well J core, which collected from within a production zone at the culmination in the boundary (Figure 3), is clearly related to the lithology of the siliceous rocks. Of the samples collected from the well J core, the quartzose porcelanites with hydrocarbon shows in the matrix (no. 11–13, 15, and 16) have lower Al_2O_3 contents (3.17–5.65%) than the quartzose porcelanite without a hydrocarbon show in the matrix (no. 17), which has an Al_2O_3 content of 9.49% (Table 3). The median pore-throat radius in the porcelanites with hydrocarbon shows (0.148–0.256 μm; average, 0.212 μm) is larger than that

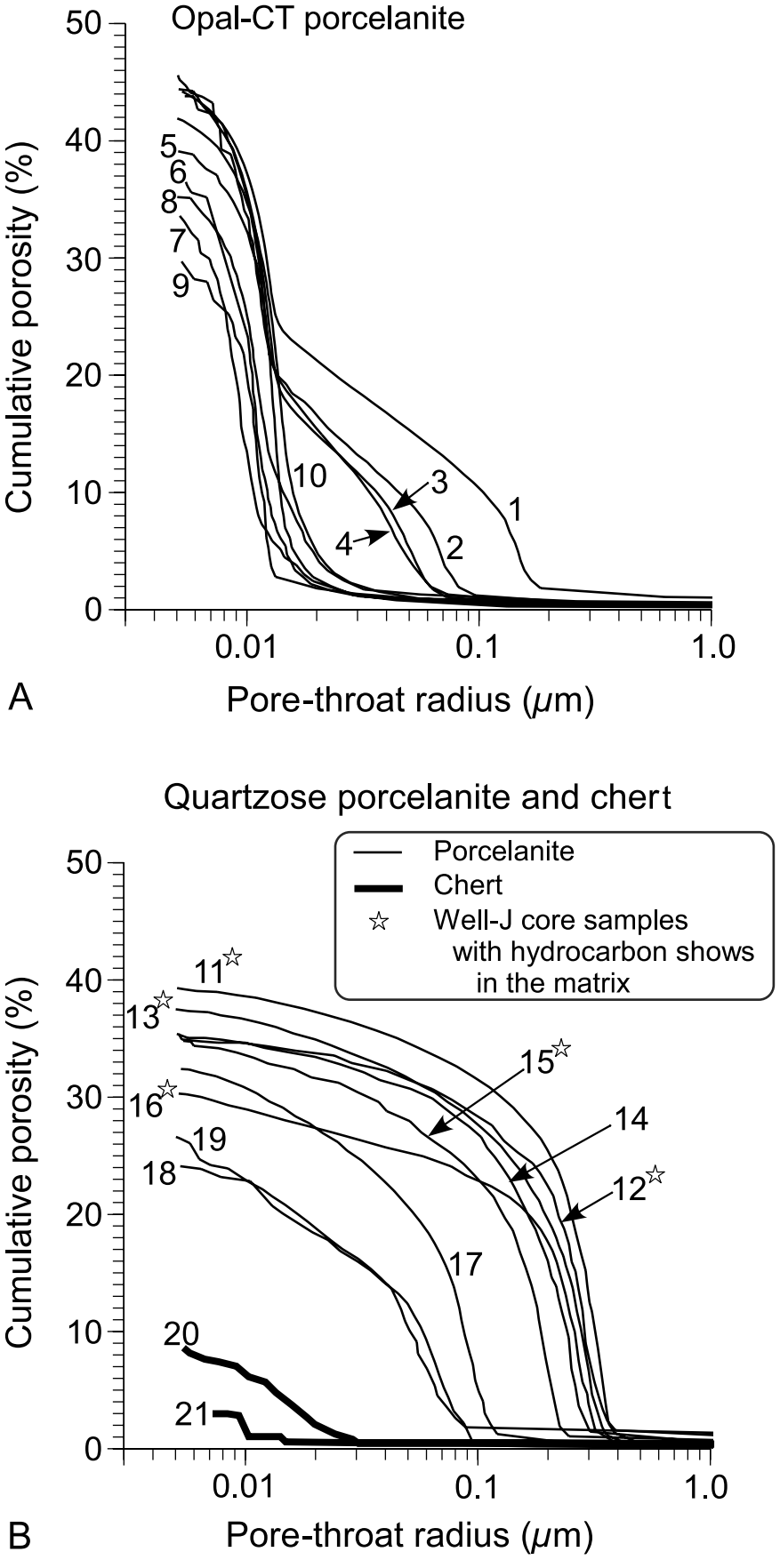

Figure 6. Distributions of pore-throat radii for porcelanite and chert samples from the Yurihara oil and gas field and neighboring outcrops. (A) Opal-CT porcelanite. (B) Quartzose porcelanite and chert. The number on each curve corresponds to the sample number listed in Table 3.

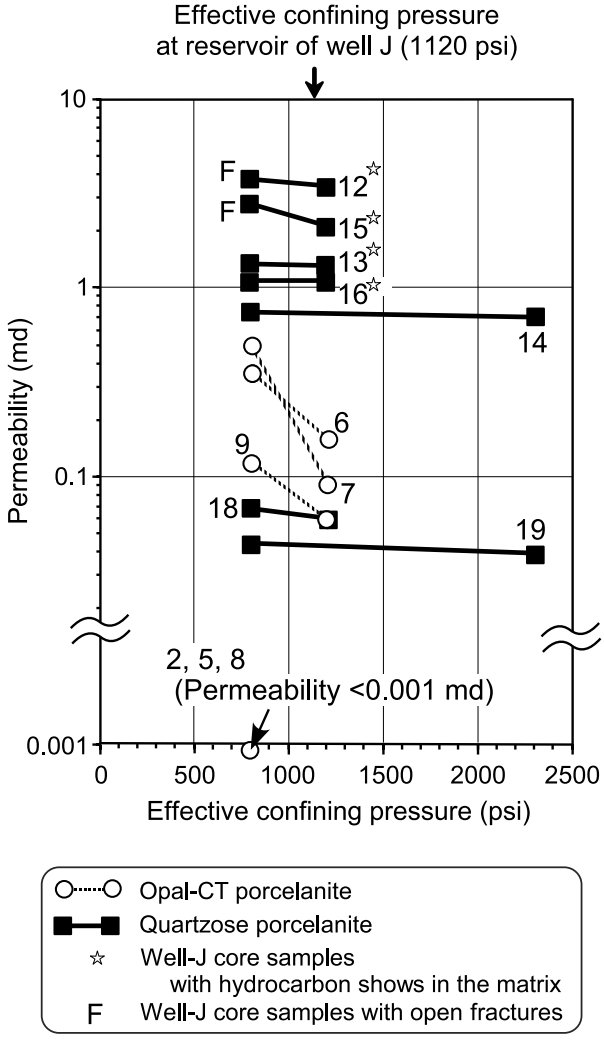

Figure 7. Relationship between permeability and effective confining pressure for porcelanite. The number on each line corresponds to the sample number listed in Table 3. Note that the permeability of sample no. 2, 5, and 8 is below the measurable limit (0.001 md) of the measuring device under an effective confining pressure of 800 psi (5.5 MPa).

in the porcelanite without the shows (0.071 μm; Table 3). The permeabilities of the former quartzose porcelanite samples without open fractures, no. 13 and 16, are 1.1 and 1.4 md, respectively, under an effective confining pressure of 800 psi (5.5 MPa). By way of comparison, these data are similar to data obtained from the oil-bearing quartzose porcelanite of the Elk Hill field (Monterey Formation) in Kern County, California, which has matrix pore radii of 0.1 to 1.0 μm and an average permeability of 0.8 md (Reid and McIntyre, 2001b).

REEXAMINATION OF DATA FROM THE TOYOTOMI AREA

Figure 9 shows the vertical trends in ϕ_{Hg}, Throat-M porosity, throat-L porosity, bulk density, and grain density at Toyotomi R-2 and Ohmagari R-1. Of the samples from the two wells, the 24 opal-CT porcelanite samples and the 36 quartzose porcelanite samples have Al_2O_3 contents ranging from 3.81 to 12.56% (Table 2). A gradual decrease in ϕ_{Hg} with increasing depth in both wells exists, with minor fluctuations, showing no abrupt change in the vicinity of the opal-CT to quartz transformation boundary. Above the boundary, the bulk and grain densities gradually increase with depth. In the Toyotomi R-2 well, however, the bulk densities of samples at depths above 400 m (1300 ft) are clearly shifted to larger values, away from the trend below, and are accompanied by localized shifts in ϕ_{Hg} to smaller values.

The porosity characteristics and distribution of pore-throat radii for porcelanite in the Toyotomi area are similar to those for porcelanite in the Yurihara area. The ϕ_{Hg} of opal-CT porcelanite ranges from 27 to 47% (average, 35%), and both unimodal and bimodal distributions are present (Table 2). The opal-CT porcelanites with a unimodal distribution have well-sorted pore radii, mostly with throat-S pores. The opal-CT porcelanites with a bimodal distribution contain throat-M and throat-L pores in addition to throat-S pores, although the combined throat-M and throat-L porosity never exceeds 16%. The ϕ_{Hg} for quartzose porcelanite, which ranges from 12 to 39% (average, 24%), is lower than that for opal-CT porcelanite. The quartzose porcelanites have a unimodal distribution, with throat-M porosity dominating. The throat-S, throat-M, and throat-L porosities are 2 to 11% (average, 6%), 1 to 23% (average, 15%), and 0 to 19% (average, 3%), respectively.

The sum of throat-M and throat-L porosity (throat-M + L porosity) can be used as an index of reservoir quality. Local increases in throat-M porosity that move in tandem with throat-L porosity occur; the throat-M + L porosity increases immediately below the transformation boundary and then steadily decreases with depth presumably because of compaction, with only minor fluctuations (Figure 9).

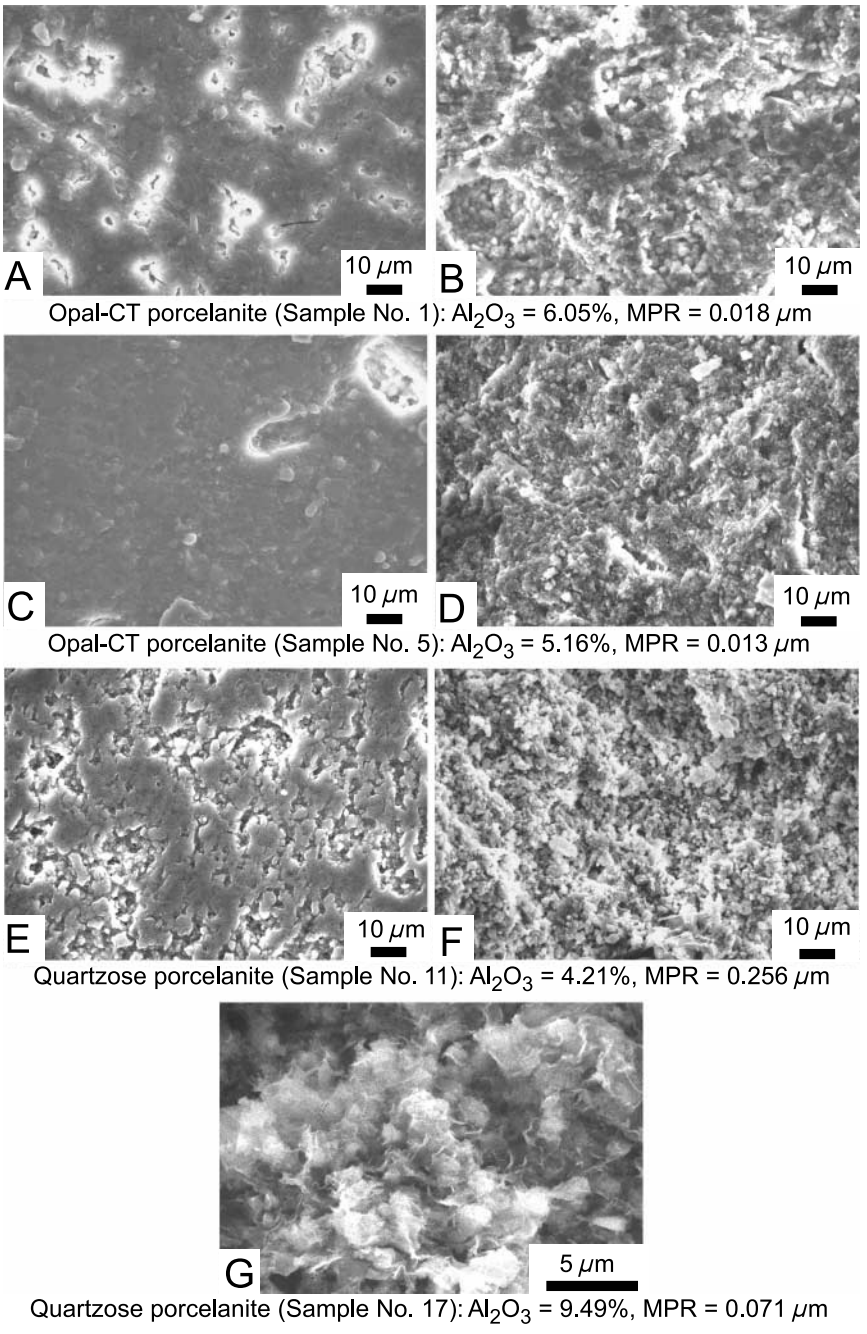

Figure 8. The SEM images of polished and artificial fractured surfaces of siliceous rocks. (A, B) Opal-CT porcelanite with a bimodal distribution of pore-throat radii (sample no.1). (C, D) Opal-CT porcelanite with a unimodal distribution of pore-throat radii (sample no. 5). (E, F) Quartzose porcelanite (sample no. 11). (G) Quartzose porcelanite (sample no. 17). (A, C, and E) Polished surface. (B, D, F, and G) Fractured surface. MPR = median pore-throat radius.

In both wells, hydrocarbon shows have been identified for many horizons; in addition, permeable zones have been inferred in certain horizons by loss of circulation during drilling (Figure 9). Production tests were conducted at four horizons in Ohmagari R-1 and at one horizon in Toyotomi R-2, confirming gas production from all horizons tested (Figure 9). Intervals of lost circulation and gas production, occurring only below the opal-CT to quartz transformation boundary, are approximately coincident with the horizons of quartzose porcelanite with throat-M + L porosity above 20% in Toyotomi R-2 and above 15% in Ohmagari R-1 (Figure 9). These horizons also lie within a zone of hydrocarbon shows. Thus, increases in throat-M + L porosity indicate improved reservoir quality.

In contrast, quartzose porcelanite with a low throat-M + L porosity may act as a seal. In places,

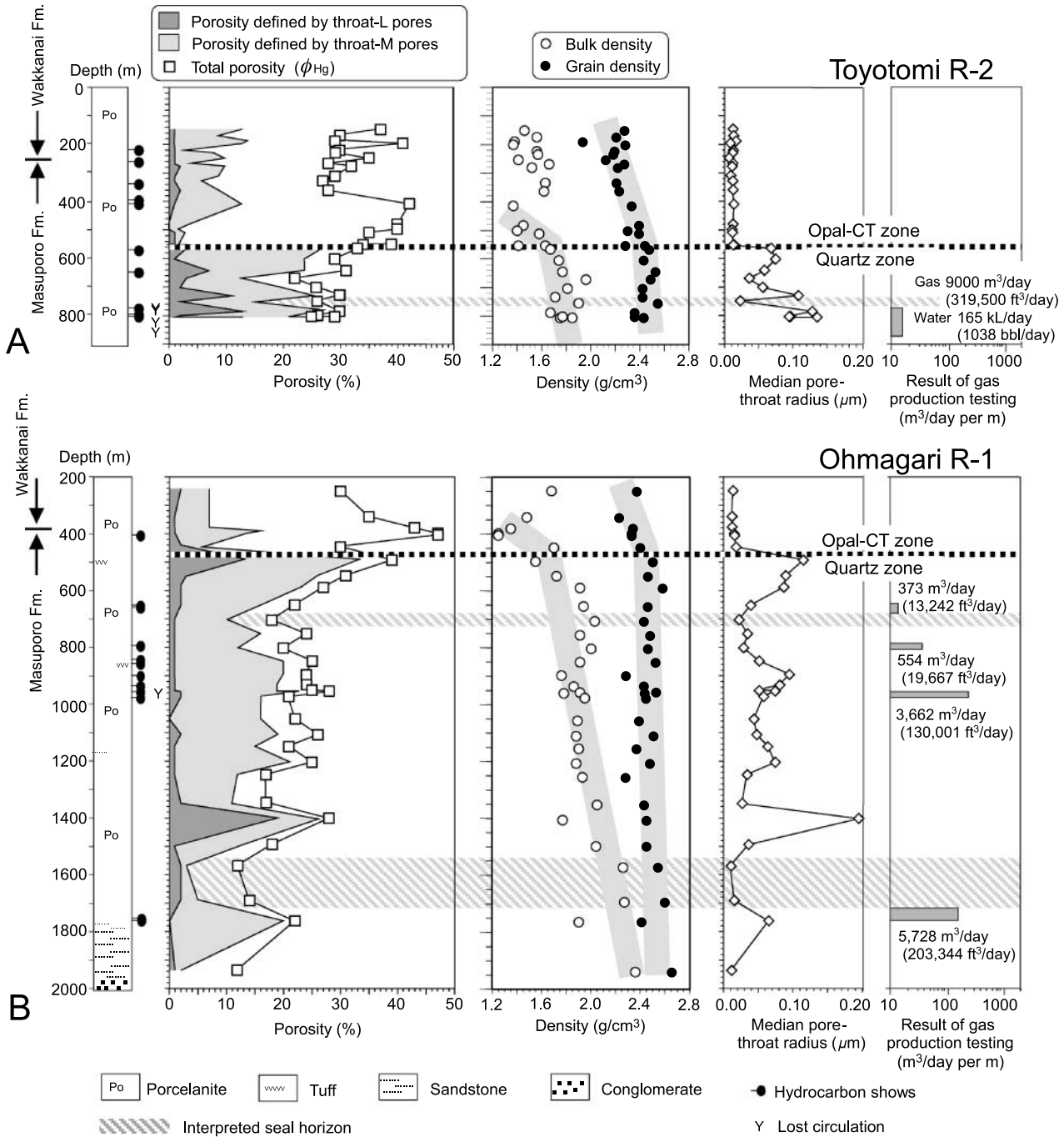

Figure 9. Plot of total porosity, throat-L (pore-throat radius ≥0.15 μm) porosity, throat-M (0.15 μm > pore-throat radius ≥ 0.02 μm) porosity, bulk density, grain density, and median pore-throat radius versus depth. A lithologic column, hydrocarbon shows, and intervals of lost circulation and gas production are also shown. The production data are shown both as a volume per day and a volume per day per depth meter. (A) Toyotomi R-2 well. (B) Ohmagari R-1 well. Note that the intervals with gas production and lost circulation correspond to those with higher throat-M + L porosity (the sum of throat-M and throat-L porosity) in quartzose porcelanite.

proven reservoir horizons are observed to be overlain by such porcelanites that have a low throat-M + L porosity and no hydrocarbon shows. These interpreted porcelanite seals are observed to have throat-M + L porosities of 15% and 3 to 10% in the Toyotomi R-2 and Ohmagari R-1, respectively (Figure 9).

Note that hydrocarbon shows have also been observed above the transformation boundary within

opal-CT porcelanite that has a bimodal distribution of pore-throat radii that is characterized by higher throat-M + L porosities (exceeding 9%) than those of surrounding layers (Table 2; Figure 9).

In both wells within the Toyotomi area, quartzose porcelanites demonstrate the highest class of throat-M + L porosity and highest level of median pore-throat radius immediately below the transformation boundary. The Yurihara field contains a hydrocarbon trap immediately below the boundary, whereas the Toyotomi area contains neither gas production nor remarkable hydrocarbon shows in this horizon.

EFFECT OF THE OPAL-CT TO QUARTZ DIAGENETIC TRANSFORMATION ON RESERVOIR PROPERTIES

Effects of the Transformation on Pores

The characteristics of pores in diagenetically altered porcelanites have been previously investigated by Tada and Iijima (1983). The throat-S pores located within the matrix of opal-CT porcelanite, which are too small to be visible in a 1000× SEM image, are equivalent to the ultramicropores described by Tada and Iijima (1983). The pores in the opal-CT porcelanites have a unimodal distribution of pore-throat radii and are mostly throat-S type (Table 3; Figure 6A). Throat-S porosity generally exceeds 30% (Tables 3, 4), although the density of pores observed in 1000× SEM images of polished surfaces is much less than that expected from the throat-S porosity (Figure 8C). We therefore assume that most of the throat-S pores occur as extremely small pores in the matrix. This is supported by the observation of ultramicropores by Tada and Iijima (1983), which had pore diameters on the order of 0.05 μm in 50,000× SEM images of the opal-CT porcelanite matrix.

By contrast, throat-M pores in the opal-CT porcelanite with a bimodal distribution of pore-throat radii are visible in 1000× SEM images and are equivalent to the macropores and micropores described by Tada and Iijima (1983). The pores in the opal-CT porcelanites with a bimodal distribution are mainly throat-S and throat-M types. The pores observable in SEM images of polished surfaces (Figure 8A) are more common than those in the opal-CT porcelanites with a unimodal distribution. Therefore, these pores are assumed to be mainly throat-M type. We assume from their shape and size that the throat-M pores are equivalent to macropores and micropores that correspond to the moldic pores of the dissolved tests of diatoms and radiolarians and intraparticle pores representing the chambers of these tests (Tada and Iijima, 1983).

In quartzose porcelanite, network pores, which have been newly generated in the matrix of opal-CT porcelanite, interconnect with larger pores that were derived from the throat-M pores found in opal-CT porcelanite. Pores in quartzose porcelanite are mainly throat-M and throat-L types (Tables 3, 4; Figure 6B). The polished surfaces of the sample reveal larger pores with diameters ranging from 5 to 10 μm as well as network pores several microns in width interconnected with the larger pores (Figure 8E). On the basis of their shape and size, we assume that the larger pores are not only equivalent to the macropores or micropores of Tada and Iijima (1983) but are derived from the throat-M pores found in opal-CT porcelanite. Accordingly, we conclude that the network pores form during the opal-CT to quartz diagenetic transformation in the apparently homogeneous matrix of opal-CT porcelanite, whose 1000× SEM image does not show pores. On the basis of the shape and size of the network pores, we assume that these pores are the equivalent of the micropores of Tada and Iijima (1983). Because artificial fractures appear to occur along larger pores, we believe that most of the fractured surfaces represent the inner walls of macropores (Figure 8F). Consequently, we assume that the pores that occur among quartz particles, as seen on fractured surfaces, are the throats of network pores (micropores).

Pore throats in clay-rich (high Al_2O_3) quartzose porcelanite are narrowed by clay minerals (Figure 8G) that probably emerged in association with the generation of network pores (Figure 8E) during diagenetic transformation. The phase transformation of silica minerals in porcelanite is a dissolution-reprecipitation process (Stein and Kirkpatrick,

1976). Opal-CT, which was located in the matrix before the transformation, dissolves to form network micropores during the transformation and reprecipitates as quartz in adjacent ultramicropores. Argillaceous clastics (mainly clay minerals) that were originally located within the matrix presumably remained behind through the transformation, and some of them emerged in the network micropores of quartzose porcelanite. However, in opal-CT porcelanite, argillaceous clastics do not affect the throat radii of throat-S pores in the matrix, which consists of homogeneous aggregates of opal-CT and argillaceous clastics (Tada and Iijima, 1983). Argillaceous clastic particles containing clay minerals are generally larger than throat-S pores; consequently, the throat radii of pores are unlikely to be affected by clay minerals. Also the clastic particles are not located within the pores (macropores or micropores) because the pores arise from the dissolution and/or the chamber structure of tests.

The textural heterogeneity caused by network pores that formed during the transformation can extend across distances of several millimeters. These network pores are several microns wide, meaning that the formation of such pores creates heterogeneity on the scale of microns. Among the analyzed samples, the ϕ_{CMS} and ϕ_{Hg} values are similar for all the opal-CT porcelanites, but the two quartzose porcelanites (no. 15 and 16) had different values. The plug cores used for the ϕ_{CMS} measurement were larger than 10 cm^3, whereas the samples analyzed for the ϕ_{Hg} measurement were smaller than 0.4 cm^3; therefore, the ϕ_{Hg} would be more susceptible to a millimeter scale of textural heterogeneity. This is the case for both of the quartzose porcelanites.

Effects of the Transformation on Permeability

Opal-CT porcelanite generally has lower permeability than quartzose porcelanite. Half of the opal-CT porcelanite samples have permeabilities below the lower limit of measurement, and the remaining samples show a marked decrease in permeability with increase in the confining pressure (Figure 7). However, the opal-CT porcelanite samples show only a minor decrease in porosity with increasing confining pressure (Figure 5). The reason for this is likely caused by the contrast in pore types and matrix ductility observed in the opal-CT and quartzose porcelanites. Opal-CT porcelanite has many more throat-S pores (Figures 6A, B; 9A, B) and greater ductility than quartzose porcelanite (Snyder et al., 1983; Chaika and Williams, 2001), thereby allowing pore throats to be narrowed under increasing pressure with only a minor drop in porosity.

The permeability of quartzose porcelanite is dependent on the content of Al_2O_3 (clay minerals). Quartzose porcelanite with low Al_2O_3 generally has fewer throat-S pores, more throat-M and throat-L pores, and higher permeability than opal-CT porcelanite. The relatively low ductility of quartzose porcelanite prevents the permeability from decreasing even under high effective confining pressures (Figure 7). Quartzose porcelanite with high Al_2O_3 has lower permeability than samples with low Al_2O_3 because the pore throats in quartzose porcelanite with high Al_2O_3 are narrowed by the clay minerals that emerged in the pores during the diagenetic transformation.

The general pattern of how the permeability changes with the effective confining pressure (Figure 7) suggests the following relationship between quartzose and opal-CT porcelanites. When the effective confining pressure is sufficiently low (as low as 500 psi [3.4 MPa]), some opal-CT porcelanites probably possess a permeability as high as those of quartzose porcelanites. However, under an effective confining pressure of approximately 1000 psi (~6.9 MPa), such an opal-CT porcelanite would have a lower permeability than quartzose porcelanite with low Al_2O_3, and under an effective confining pressure of more than 1500 psi (10.3 MPa), its permeability would be lower than that of quartzose porcelanite with high Al_2O_3 (Figure 7).

In some opal-CT porcelanite, permeabilities have been observed to be as high as in quartzose porcelanite. Under normal conditions, the permeability of opal-CT porcelanite, which is dominated by throat-S pores, should be different from that of quartzose porcelanite, which is dominated by throat-M and throat-L pores. However, previous studies have reported the development of

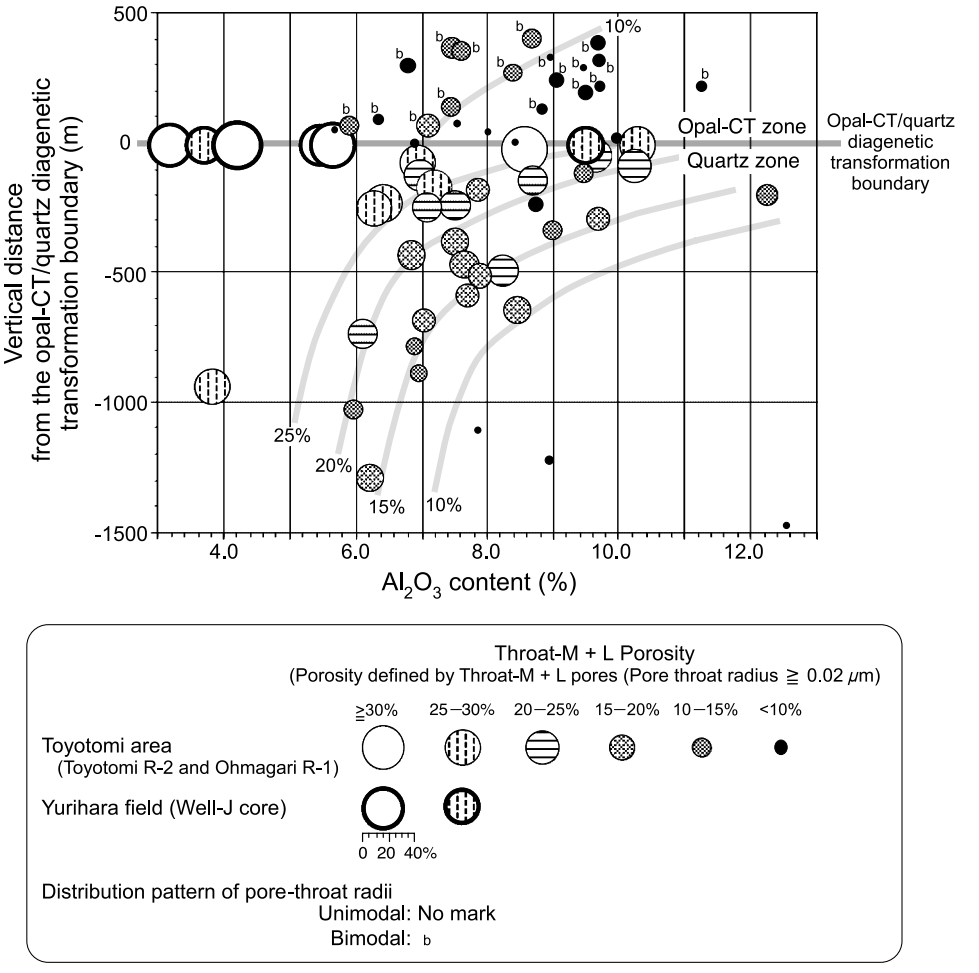

Figure 10. Relationships among throat-L + M (pore-throat radius ≥0.02 μm) porosity, Al_2O_3 content, and depth from the opal-CT to quartz transformation boundary for porcelanite in the Toyotomi area and the Yurihara oil and gas field. Note that throat-L + M porosity decreases with increasing Al_2O_3 content and burial depth, in both the quartz and opal-CT zones. See text for further details.

microfractures in porcelanite (Montgomery and Morea, 2001; Reid and McIntyre, 2001a) that could greatly increase permeability. That said, the opal-CT porcelanite in this study shows a rapid decrease in permeability with increasing confining pressure (Figure 7) that again suggests that such microfractures can be effectively closed under a sufficiently high confining pressure.

Effects of the Transformation on Throat-M + L Porosity

As previously mentioned, we found that throat-M + L porosity can be used to map reservoir quality as it is affected by diagenesis and burial depth. The pore properties of siliceous rocks are also dependent on clay content (Iijima and Tada, 1981; Goter et al., 1992; Tsuji and Yokoi, 1994; Chaika and Williams, 2001; Reid and McIntyre, 2001a).

Therefore, we examine the relationships between throat-M + L porosity, Al_2O_3 (clay) content, and burial depth (Figure 10). Here, the burial depth is expressed as the vertical distance from the diagenetic transformation boundary to compare properties of porcelanites between two areas that have different geologic/burial histories. Throat-M + L porosity shows an abrupt increase immediately below the boundary. Both above and below the boundary, throat-M + L porosity has a negative correlation with both burial depth and Al_2O_3 content. We explain this relationship in terms of the following factors: (1) the pore throats in porcelanite expand during the transformation; (2) as the burial depth increases, both opal-CT porcelanite and quartzose porcelanite undergo mechanical compaction with little cementation (Tada and Iijima, 1983; Tada, 1991a); (3) clay minerals enhance the ductility of porcelanite (Tada and Siever, 1989) and facilitate its compaction (Tada and Iijima, 1983);

and (4) during the transformation, some of the clay minerals emerge in the network pores, narrowing the pore-throat radii, particularly in the case of quartzose porcelanite rich in argillaceous clastics (Al_2O_3).

On the basis of the previous findings, we plot lines of equal throat-M + L porosity in Figure 10. The slopes of these lines suggest that the rate of reduction in throat-M + L porosity with increasing burial depth is strongly dependent on the Al_2O_3 content. The slopes of the lines of equal throat-M + L porosity of 10 to 25% are steep when the Al_2O_3 content is less than 5 to 8%, meaning that the burial depth does not affect the porosity as much. At higher Al_2O_3 contents, the slope is gentler, meaning that the burial depth greatly affects the porosity.

FORMATION OF HYDROCARBON TRAPS

We propose the following process for the formation of hydrocarbon traps in porcelanite reservoirs. Under a sufficiently high confining pressure, the most impermeable porcelanite (i.e., one that is highly suitable as a seal) is the clay-rich (high Al_2O_3) opal-CT porcelanite located immediately above the diagenetic boundary. Conversely, the most permeable porcelanite (i.e., one that is rich in pores that can hold hydrocarbons and is highly suitable as a reservoir) is the clay-poor (low Al_2O_3) quartzose porcelanite located immediately below the boundary. In other words, the former corresponds to the most compacted opal-CT porcelanites and the latter corresponds to the least compacted quartzose porcelanites. In this scenario, seals and reservoirs occur immediately above and below the transformation boundary, respectively. With the addition of a closing structure of any kind, a trap would be formed.

This model explains the formation of reservoir and seal in the Yurihara field (Figures 2, 3), where the transformation boundary is as deep as 1250 to 1400 m (4100–4600 ft) below ground (–994 to –1141 m asl [–3261 to –3743 ft asl]). When Waseda and Iwano (2007) measured the carbon isotope compositions of gases adsorbed by drill cuttings in the Yurihara field, they found a marked shift to heavier values immediately below the boundary. This observation strongly supports the proposal that the opal-CT porcelanite located immediately above the boundary is acting as a seal.

As previously mentioned, the permeability of some opal-CT porcelanites comes close to that of quartzose porcelanites under low confining pressure. In the Toyotomi area, the transformation boundary is as shallow as approximately 500 m (~1650 ft) below ground (Figure 9). In this case, the shallow depth of the boundary prevents the opal-CT porcelanite from acting as an effective seal. This explains why the quartzose porcelanite located immediately below the boundary contains no hydrocarbons, despite a high throat-M + L porosity (exceeding 20%) (Figure 9). When such a horizon with high throat-M + L porosity is intercalated with a clay-rich quartzose porcelanite, the latter material can form a seal. Moreover, this scenario explains why hydrocarbon shows occur above the transformation boundary in horizons that have higher throat-M + L porosities (>9%) than the surrounding layers (Figure 9). These shows can be interpreted as hydrocarbons that migrated upward through nonsealing opal-CT porcelanite layers with high throat-M + L porosities. This provides a suitable explanation for the occurrence of hydrocarbons in the Toyotomi area (Figure 9).

PROPOSAL OF NEW HYDROCARBON TRAP MODELS

In line with our proposed process for the formation of hydrocarbon traps, we propose two new trap models. Because an example of one such trap is seen in the Yurihara field and an example of the other is seen in the Toyotomi area, we will refer to the trap models as the Yurihara model and the Toyotomi model.

We start by noting that the reservoir units are common to both fields. The reservoirs consist of quartzose porcelanites that are poor in clay minerals (Al_2O_3) and have moderately high throat-M + L porosity. As previously mentioned, in the Yurihara field, the throat-M + L porosity of the hydrocarbon-bearing quartzose porcelanites from the well J core is greater than 27% (Table 3).

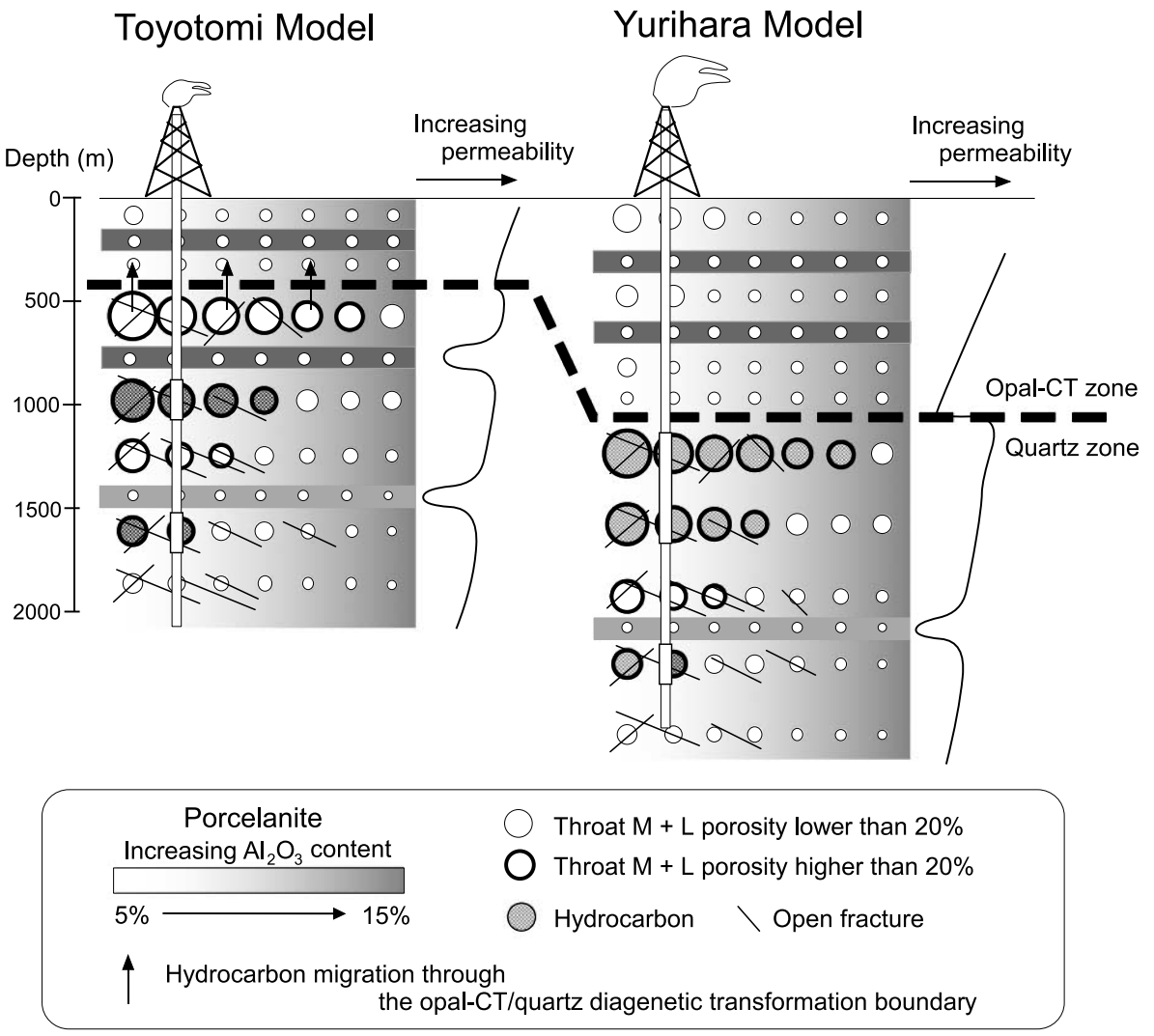

Figure 11. Schematic diagrams of two new models of hydrocarbon traps in siliceous rock. The intercalation of clay-rich porcelanite in a Yurihara model can lead to the formation of a Toyotomi model, resulting in the coexistence of the two models (the lowest part of the Yurihara model). Symbol size (circles) scales with throat-M + L porosity (%).

Quartzose porcelanites that host gas production and hydrocarbon shows in the Toyotomi field have throat-M + L porosities greater than 20 and 15% in the Toyotomi R-2 and Ohmagari R-1 wells, respectively (Figure 9). Given these values, we assume that quartzose porcelanite with a throat-M + L porosity exceeding 20% provides a good reservoir.

The seals in these two fields are of different lithologic types because the permeability of opal-CT porcelanite changes markedly with changes in the confining pressure (Figure 7). If opal-CT porcelanite is to function effectively as a seal, we have suggested that it requires an effective confining pressure on the order of 1000 psi (6.9 MPa), which is equivalent to a depth of approximately 1000 m (~3300 ft). This value lies between two effective confining pressures: 1120 psi (7.7 MPa) at the gas-producing zone (a mean depth of 1310 m [4300 ft]) close to the transformation boundary of the Yurihara field where opal-CT porcelanite acts as a seal, and 500 psi (3.4 MPa) estimated at the boundary (at a depth of ~500 m [~1650 ft]) in the Toyotomi area where opal-CT porcelanite does not act as a seal. This assumed cutoff pressure is consistent with the relationship between permeability and effective confining pressure, as shown in Figure 7. Horizons interpreted as seals in Toyotomi-type traps have throat-M + L porosity values of 3 to 15%

(Figure 9). Thus, we conclude that quartzose porcelanite with throat-M + L porosities below 10% can act as a seal.

From the previous discussion, we have developed two trapping models (Figure 11). In our Yurihara model, opal-CT porcelanite located immediately above the transformation boundary acts as a seal, and quartzose porcelanite that is located beneath the transformation boundary and has a throat-M + L porosity greater than 20% forms reservoirs. The lines of equal throat-M + L porosity in Figure 10 indicate that quartzose porcelanite located immediately below the boundary meet this requirement (i.e., throat-M + L porosity exceeding 20%) as long as the Al_2O_3 content is below 11%. At 1000 m (3300 ft) below the boundary, the requirement for a suitable reservoir is an Al_2O_3 content of less than 6% (Figure 10).

In our Toyotomi model, the transformation boundary observed at approximately 500 m (~1650 ft) is too shallow for the opal-CT porcelanite to act as a seal. However, in the situation where clay-rich (high Al_2O_3) porcelanite with a throat-M + L porosity less than 10% intercalated with quartzose porcelanite that meets the same reservoir requirements as the Yurihara model is present, hydrocarbons can be stratigraphically or structurally trapped within the reservoir rock. For quartzose porcelanite to form this type of a seal, it must have an Al_2O_3 content more than 15% if located immediately below the boundary and more than 8% at a depth of 1000 m (3300 ft) below the boundary (Figure 10).

The intercalation of clay-rich porcelanite in a Yurihara model can lead to the formation of a Toyotomi model, resulting in the coexistence of the two models (Figure 11).

POSSIBILITY OF SIMULTANEOUS DEVELOPMENT OF MATRIX PORES AND FRACTURES

More than 50 yr of gas production from the Toyotomi gas field attest to the substantial resource potential of matrix porosity in siliceous rocks. The Toyotomi R-2 well, drilled in 1947, produced 4000 to 6000 m^3 (142–213 mcf) gas/day until production stopped in 1972 because of well problems (Hokkaido Government, 1969). The Toyotomi R-1 well, drilled in 1925, produced more than 10,000 m^3 (355 mcf) gas/day until 1975 (Hokkaido Government, 1969).

Porcelanite with well-developed matrix porosity is also potentially prone to the development of fractures. Because the formation of fractures depends on the ductility of rocks under equal stress and strain conditions, greater numbers of fractures are expected to form in quartzose porcelanite with relatively low clay (Al_2O_3) content, and accordingly, a high throat-M + L porosity. This is consistent with the fact that zones of lost circulation in the Toyotomi area coincide with horizons of high throat-M + L porosity. Such well-developed fractures possibly caused the loss in circulation and led to enhanced gas productivity. This conjecture is supported by the finding of Reid and McIntyre (2001a) that clay-poor porcelanite contains a higher fracture density than clay-rich porcelanite and by the results of Goter et al. (1992) that siliceous rock with a "clean" quartz phase has superior reservoir properties and that such reservoirs have a double porosity system (i.e., matrix and fracture porosity).

Note some of the differences between the reservoir properties of porcelanite and chert, which is the main lithologic type involved with fractured reservoirs in the Monterey Formation. Chert is more brittle than porcelanite (Snyder et al., 1983) and contains a higher density of fractures for a given degree of diagenesis. As the Onnagawa Formation in the Yurihara field also contains quartzose chert, and more fractures develop in the chert in the well J core than in quartzose porcelanite, we assume that this would enhance the productivity of the reservoirs containing quartzose chert.

APPLICABILITY OF THE CHAIKA AND WILLIAMS (2001) CLASSIFICATION SCHEME FOR SILICEOUS ROCK RESERVOIRS

Chaika and Williams (2001) showed that matrix- and fracture-porosity–dominated reservoirs in the siliceous rocks of the Monterey Formation have

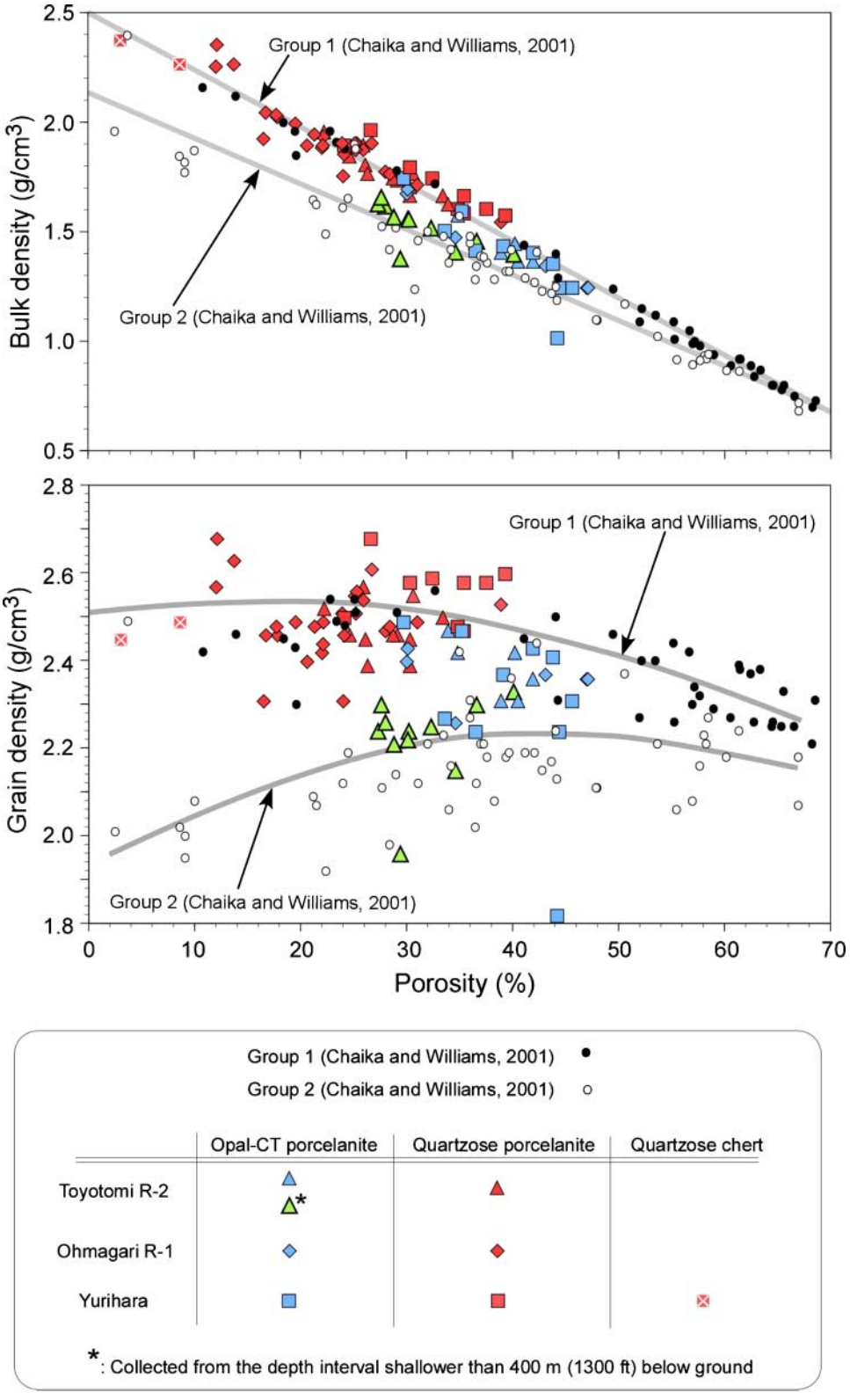

Figure 12. Relationships between bulk density or grain density and porosity for core and/or outcrop data from the Yurihara and Toyotomi areas.

characteristic ratios of bulk density to porosity. They demonstrated that group 1 reservoirs (with higher ratios) and group 2 reservoirs (with lower ratios) mostly coincide with matrix-porosity–dominated and fracture-porosity–dominated reservoirs, respectively. They assumed that the former have a higher content of clay minerals than the latter.

To evaluate the applicability of the Chaika and Williams (2001) classification to siliceous rocks in Japan, we plotted the data in the same way that they did (Figure 12). As can be seen, all of the quartzose porcelanites and cherts, and some of the opal-CT porcelanites, are coincident with group 1, whereas the rest of the opal-CT porcelanites are coincident with group 2. Accordingly, we assign the matrix-porosity–dominated reservoirs in this study into group 1 (Figure 12) (cf. Monterey Formation reservoirs from Chaika and Williams, 2001).

The clay content in samples assigned to the two groups is not always consistent with Chaika and Williams (2001). For example, the samples assigned to groups 1 and 2 in this study have similar Al_2O_3 contents (average values, 7.52 and 7.77%, respectively). Furthermore, the Al_2O_3 content of the opal-CT porcelanite samples from Toyotomi R-2 is 7.83% for group 1 and 8.81% for group 2. This relationship is contrary to the conclusions of Chaika and Williams (2001). Here, groups 1 and 2 are defined as having grain densities more than 2.35 g/cm^3 and less than 2.30 g/cm^3, respectively.

The difference between groups 1 and 2 presumably results from the difference in the degree of opal-CT cementation. Most of the group 2 samples consist of opal-CT porcelanite collected at depths above 400 m (1300 ft) in Toyotomi R-2 (Figure 12). As previously stated, these porosities (ϕ_{Hg}) on average are lower than those of opal-CT porcelanite samples from greater depths (Figure 9). The extent of cementation at depths above 400 m (1300 ft) can cause these shifts. Tada and Iijima (1983) demonstrated that siliceous rock exposed at the surface in Japanese examples has generally been transformed into opal-CT chert by tridymite cement precipitated from groundwater. The water chemistry observed in six wells located between Toyotomi R-2 and Ohmagari R-1 indicates infiltration of meteoric water to depths of 100 to 400 m (330–1300 ft) (Ishii et al., 2007). Thus, group 2 samples possibly have been cemented by opal-CT. Considering this, a possibility exists that for the samples in this study, group 2 initially may have contained more Al_2O_3 than group 1. Accordingly, the differences between the two reservoir types are highly unlikely to reflect different initial compositions, as suggested by Chaika and Williams (2001); instead, they reflect the extent of cementation related to the infiltration of meteoric water.

CONCLUSIONS

We have examined the changes in petrophysical properties that accompanied the diagenetic transformation of siliceous rock in the Yurihara field and the Toyotomi area, and reached several conclusions.

1. As diagenetic transformation turns opal-CT into quartz, the throat radii of porcelanite pores abruptly increase and ductility decreases, accompanied by a gradual decrease in the porosity because of compaction during burial.
2. An increase in clay (Al_2O_3) content causes an increase in the ductility of the porcelanite and facilitates a reduction in the throat radii with burial compaction.
3. In clay-rich (high Al_2O_3) quartzose porcelanite, clay minerals, which emerge in the network pores generated by the opal-CT to quartz diagenetic transformation, reduce the throat radii of pores.
4. Under high effective confining pressures at depths deeper than approximately 1000 m (~3300 ft), the permeability of clay-poor (low Al_2O_3) quartzose porcelanite is generally higher than that of opal-CT porcelanite. However, under lower effective confining pressures at depths shallower than 500 m (~1650 ft), some opal-CT porcelanites can have permeabilities comparable to those of quartzose porcelanite.

Correlation of these characteristics with the occurrence of hydrocarbons led us to the development of the following trap models.

Yurihara Model: When the opal-CT to quartz diagenetic transformation boundary is deeper than

approximately 1000 m (~3300 ft) below ground, opal-CT porcelanite immediately above the boundary forms seals and clay-poor quartzose porcelanite immediately below the boundary forms reservoirs. Structural closure of any kind then results in hydrocarbon traps. When quartzose porcelanite contains less than 6% Al_2O_3, it has the potential to form reservoirs in the 1000-m (3300-ft)-thick interval below the boundary.

Toyotomi Model: When the diagenetic transformation boundary is shallower than ~500 m (1650 ft) belowground, opal-CT porcelanite located immediately above the boundary does not always act as a seal. However, as is the case with the Yurihara model, reservoirs composed of clay-poor quartzose porcelanite are still common. When clay-rich quartzose porcelanite is intercalated in such a horizon, it forms seals, thereby forming hydrocarbon traps. In this type of seal, the Al_2O_3 content must exceed 15% at the level of the transformation boundary or 8% at a depth of 1000 m (3300 ft) below the boundary.

These two newly defined models both present traps consisting of quartzose porcelanite reservoirs with well-developed matrix porosities. These models might prove useful in exploring porcelanite in similar siliceous rock formations, such as the Monterey Formation in California.

REFERENCES CITED

Aoyagi, K., and T. Kazama, 1980, Transformational changes of clay minerals, zeolites and silica minerals during diagenesis: Sedimentology, v. 27, p. 179–188, doi:10.1111/j.1365-3091.1980.tb01168.x.

Araki, N., and S. Kato, 1993, A discovery of the Ayukawa oil and gas field, Akita Prefecture: Journal of the Japanese Association for Petroleum Technology, v. 58, p. 119–127.

Chaika, C., and L. A. Williams, 2001, Density and mineralogy variations as a function of porosity in Miocene Monterey Formation oil and gas reservoirs in California: AAPG Bulletin, v. 85, p. 149–167.

Fukusawa, H., K. Hoyanagi, and M. Akiyama, 1992, Stratigraphic and paleoenvironmental study of the Neogene formations in northern central Hokkaido, Japan (in Japanese with English abstract), *in* I. Kobayashi, M. Tateishi, K. Takayasu, Y. Matoba, and M. Akiyama, eds., The Neogene in the eastern margin of the paleo-Sea of Japan: Stratigraphy paleogeography paleoenvironment: Memoir of the Geological Society of Japan 37, p. 1–10.

Garrison, R. E., 1975, Neogene diatomaceous sedimentation in East Asia: A review with recommendations for further study: Coordination of Joint Prospecting for Mineral Resources in Asian Offshore Areas, Technical Bulletin 9, p. 57–69.

Goter, E. R., M. G. Picha, M. A. Sandstorm, and D. E. Schwartz, 1992, A new geological reservoir model for the Monterey: An alternative to the "fractured shale" model (abs.): AAPG Annual Meeting, p. 47–48.

Hokkaido Government, 1969, Oil and natural gas resources in Hokkaido (in Japanese): Japan Natural Gas Association, 205 p.

Iijima, A., 1992, Evolution of Tertiary sedimentary basins of Japan in reference to rifting of the Japan Sea: Journal of the Japanese Association for Petroleum Technology, v. 57, p. 171–179.

Iijima, A., and R. Tada, 1981, Silica diagenesis of Neogene diatomaceous and volcaniclastic sediments in northern Japan: Sedimentology, v. 28, p. 185–200, doi:10.1111/j.1365-3091.1981.tb01676.x.

Inaba, M., 2001, Basalt reservoir in the Yurihara oil and gas field, northern Japan (in Japanese with English abstract): Journal of the Japanese Association for Petroleum Technology, v. 66, p. 56–67.

Ishii, E., K. Hama, T. Kunimaru, and H. Sato, 2007, Change in groundwater pH by infiltration of meteoric water into shallow part of marine deposits (in Japanese with English abstract): Journal of Geological Society of Japan, v. 113, p. 41–52.

Japan Natural Gas Association and Japan Offshore Petroleum Development Association, 1982, Oil and natural gas resources in Japan (in Japanese): Japan Natural Gas Association, 455 p.

Masui, Y., and T. Tsuji, 1990, Petroleum geology of siliceous shale of the Onnagawa Formation distributed around the Yurihara oil and gas field (Japanese abstract): Journal of the Japanese Association for Petroleum Technology, v. 55, p. 285.

Montgomery, S. L., and M. F. Morea, 2001, Antelope shale (Monterey Formation), Buena Vista Hills field: Advanced reservoir characterization to evaluate CO_2 injection for enhanced oil recovery: AAPG Bulletin, v. 85, p. 561–585.

Nagano, S., 1960, Geology of Toyotomi district with geological sheet map at 1: 50,000 (in Japanese with English abstract): Geological Survey of Hokkaido, 42 p.

Ozawa, A., T. Katahira, S. Nakano, N. Tsuchiya, and Y. Awata, 1988, Geology of Yashima district with geological sheet map at 1: 50,000 (in Japanese with English abstract): Geological Survey of Japan, 87 p.

Reid, S. A., and J. L. McIntyre, 2001a, Monterey Formation porcelanite reservoirs of the Elk Hills field, Kern County, California: AAPG Bulletin, v. 85, p. 169–189.

Reid, S. A., and J. L. McIntyre, 2001b, Geologic controls on petroleum production from the Monterey Formation quartz-phase porcelanite reservoirs, Elk Hills field, Kern County, California (abs.): AAPG Annual Meeting Expanded Abstracts, v. 10, p. 165.

Rogers, J. P., and M. W. Longman, 2001, An introduction to chert reservoirs of North America: AAPG Bulletin, v. 85, p. 1–5.

Sato, O., and S. Annaka, 1986, Reservoir petrography of volcanic rocks from the Shin-Kurokawa-1 well in the Akita oil fields, northeast Japan (in Japanese with English abstract), *in* J. Aiba, T. Asakawa, K. Sasaki, S. Sato, I. Shimada, K.Sekiguchi, and Y. Fujita, eds., Contributions to petroleum geoscience: Prof. K. Taguchi Memorial Volume: Prof. K. Taguchi Taikan Kinenkai, p. 137–148.

Sato, O., R. Furukawa, and Y. Takai, 1979, Mudstone consists of quartz particles (Japanese abstract): Journal of the Japanese Association for Petroleum Technology, v. 44, p. 40.

Schwalbach, J., S. Gordon, C. O'Brien, B. Benmore, and C. Huggins, 2004, Variation and complexity: Monterey Formation reservoirs of California (abs.): AAPG Meeting, Pacific Section, SEPM and SEG, v. 13, p. 126, http://www.searchanddiscovery.net/documents/abstracts/2004pacific/index.htm (accessed September 2010).

Shiraishi, T., and Y. Matoba, 1992, Neogene paleogeography and paleoenvironment in Akita and Yamagata Prefecture, Japan Sea side of northern Honshu, Japan (in Japanese with English abstract), *in* I. Kobayashi, M. Tateishi, K. Takayasu, Y. Matoba, and M. Akiyama, eds., The Neogene in the eastern margin of the paleo-Sea of Japan: Stratigraphy paleogeography paleoenvironment: Memoir of the Geological Society of Japan 37, p. 39–51.

Snyder, W. S., H. K. Brueckner, and R. A., Schweickert, 1983, Deformational system in the Monterey Formation and other siliceous sedimentary rocks, *in* C. M. Issacs and R. E. Garrison, eds., Petroleum generation and occurrence in the Miocene Monterey Formation, California: Pacific Section, SEPM, p. 151–170.

Stein, C. L., and R. J. Kirkpatrick, 1976, Experimental porcelanite recrystallization kinetics: A nucleation and growth model: Journal of Sedimentary Petrology, v. 46, p. 430–435.

Tada, R., 1991a, Compaction and cementation in siliceous rocks and their possible effect on bedding enhancement, *in* G. Einsele, W. Ricken, and A. Seilacher, eds., Cycle and event in stratigraphy: Berlin, Springer-Verlag, p. 480–491.

Tada, R., 1991b, Origin of rhythmical bedding in middle Miocene siliceous rocks of the Onnagawa Formation, northern Japan: Journal of Sedimentary Petrology, v. 61, p. 1123–1145.

Tada, R., and A. Iijima, 1983, Petrology and diagenetic changes of Neogene siliceous rocks in northern Japan: Journal of Sedimentary Petrology, v. 53, p. 911–930.

Tada, R., and R. Siever, 1989, Pressure solution during diagenesis: A review: Annual Review of Earth and Planetary Sciences, v. 17, p. 89–118, doi:10.1146/annurev.ea.17.050189.000513.

Tsuji, T., and Y. Masui, 1992, Reservoir quality of siliceous sediments controlled by diagenesis and lithology in the Yurihara oil and gas field, northern Japan (abs.): 29th International Geographical Congress Abstracts, p. 336.

Tsuji, T., and S. Yokoi, 1994, Hydrocarbon trap in the Neogene siliceous rocks in northern Hokkaido, Japan (in Japanese with English abstract): Journal of the Japanese Association for Petroleum Technology, v. 59, p. 283–295.

U.S. Geological Survey, 1974, Proposed plan of development, Santa Ynez Unit, Santa Barbara Channel, off California: Final environmental statement: U.S. Geological Survey FES 74-20, v. 1, p. II-118–II-174.

Waseda, A., and H. Iwano, 2007, Reservoir evaluation using carbon isotope composition of gas (in Japanese with English abstract): Journal of the Japanese Association for Petroleum Technology, v. 72, p. 585–593, doi:10.3720/japt.72.585.